



Published in final edited form as:

Nat Genet. 2024 February ; 56(2): 258–272. doi:10.1038/s41588-023-01626-1.

Integrative functional genomic analyses identify genetic variants influencing skin pigmentation in Africans

Yuanqing Feng¹, Ning Xie¹, Fumitaka Inoue^{2,3,4}, Shaohua Fan^{1,5}, Joshua Saskin⁶, Chao Zhang¹, Fang Zhang¹, Matthew E. B. Hansen¹, Thomas Nyambo⁷, Sununguko Wata Mpoloka⁸, Gaonyadiwe George Mokone⁹, Charles Fokunang¹⁰, Gurja Belay¹¹, Alfred K. Njamnshi¹², Michael S. Marks¹³, Elena Oancea⁶, Nadav Ahituv^{2,3}, Sarah A. Tishkoff^{1,14,15,*}

¹Department of Genetics, University of Pennsylvania, Philadelphia, PA 19104, USA.

²Department of Bioengineering and Therapeutic Sciences, University of California San Francisco, San Francisco, CA 94158, USA

³Institute for Human Genetics, University of California San Francisco, San Francisco, CA 94158, USA

⁴Present address: Institute for the Advanced Study of Human Biology (WPI-ASHBi), Kyoto University, Kyoto, 606-8501, Japan

⁵Present address: Human Phenome Institute, School of Life Science, Fudan University, Shanghai, China

⁶Department of Neuroscience, Brown University, Providence, RI 02912, USA

⁷Department of Biochemistry and Molecular Biology, Hubert Kairuki Memorial University, Dar es Salaam, Tanzania

⁸Department of Biological Sciences, Faculty of Sciences, University of Botswana, Gaborone, Botswana

⁹Department of Biomedical Sciences, University of Botswana, Gaborone, Botswana

¹⁰Department of Pharmacotoxicology and Pharmacokinetics, Faculty of Medicine and Biomedical Sciences, The University of Yaoundé I, Yaoundé, Cameroon

¹¹Department of Biology, Addis Ababa University, Addis Ababa, Ethiopia

*Corresponding author. tishkoff@pennmedicine.upenn.edu.

Author contributions

YQ.F., S.A.T. designed the study and wrote the original draft. YQ.F. performed the Hi-C, H3K27ac HiChIP, CRISPR, RNA-Seq, ATAC-Seq, CUT&RUN experiments and related data analysis. YQ.F. and F.I. conducted the MPRA under supervision of N.A., YQ.F. and C.Z. analyzed the MPRA data. SH. F. and M.H. played a role in quality control and analysis of WGS and SNP array data. YQ. F and SH. F conducted the GWAS and Di analysis. YQ.F. and N.X. performed CRISPR-editing and related assays in MNT-1. S.A.T., T.N., S.W.M., G.G.M., A.K.N., C.F., G.B. played a role in collecting data from Africa. J.S. and E.O. performed the CYB561A3 immunofluorescence imaging and analyses. E.O. and M.S. provided resources and additional experimental insights. All authors assisted with manuscript review and editing. S.A.T. supervised the project.

Declaration of interests

N.A. is an equity holder of Encoded Therapeutics, a gene regulation therapeutics company and is a co-founder and scientific advisor of Regal Therapeutics and Neomer Diagnostics. The remaining authors declare no competing financial interests.

Code availability

Public software and packages were used following developer's manuals. The custom code used for data analysis has been deposited at Github (https://github.com/fengyq/nature_genetics_codes).

¹²Brain Research Africa Initiative (BRAIN); Neuroscience Lab, Faculty of Medicine and Biomedical Sciences, The University of Yaoundé I, Department of Neurology, Central Hospital Yaoundé; Yaoundé, Cameroon

¹³Department of Pathology and Laboratory Medicine, Children's Hospital of Philadelphia Research Institute, Philadelphia, PA 19104, USA.

¹⁴Department of Biology, University of Pennsylvania, Philadelphia, PA 19104, USA.

¹⁵Center for Global Genomics and Health Equity, University of Pennsylvania, Philadelphia, PA 19104, USA.

Abstract

Skin color is highly variable in Africans, yet little is known about the underlying molecular mechanism. We applied massively parallel reporter assays to screen 1,157 candidate variants influencing skin pigmentation in Africans and identified 165 SNPs showing differential regulatory activities between alleles. Combining Hi-C, CRISPR-based editing, and melanin assays, we identified regulatory elements for *MFS12*, *HMG20B*, *OCA2*, *MITF*, *LEF1*, *TRPS1*, *BLOC1S6*, and *CYB561A3* that impact melanin levels *in vitro* and modulate human skin color. We found that independent mutations in an *OCA2* enhancer contribute to the evolution of human skin color diversity and detect signals of local adaptation at enhancers of *MITF*, *LEF1* and *TRPS1* which may contribute to the light skin color of southern Khoesan-speaking populations. Additionally, we identified *CYB561A3* as a novel pigmentation regulator that impacts genes involved in oxidative phosphorylation and melanogenesis. These results provide insights into the mechanisms underlying human skin color diversity and adaptive evolution.

Human skin color displays remarkable diversity across different populations and is hypothesized to be an adaptation to solar ultraviolet radiation ^{1,2}. Recent genome-wide association studies (GWAS) have shed light on the genetic basis of human skin color variation ³⁻¹². However, there have been relatively few GWAS in ethnically diverse Africans ^{5,13} despite the high levels of variation in skin pigmentation in Africa. Indeed, the genetic basis and evolutionary history of skin color in the Khoesan-speaking populations from Southern Africa (San), who have the oldest genetic lineages and the most lightly pigmented skin observed in Africa ^{5,13}, remain an enigma. Additionally, only a few of the candidate variants associated with human skin pigmentation have been thoroughly investigated through functional experiments ¹⁴⁻¹⁷. Furthermore, previous functional studies mainly focused on variants identified in Europeans, and the molecular mechanisms underlying skin color diversity in diverse Africans are still poorly defined ^{5,13}.

Here, we utilized functional genomics to identify new regulatory variants and genes that influence skin pigmentation in geographically and ethnically diverse Africans. We first selected 29,419 candidate variants, comprised of 9,913 variants identified from genome-wide association studies (GWAS) of African skin color ¹³, and 19,553 genetic variants showing extreme allele frequency differences between the lightly pigmented Khoesan-speaking populations (San) and other darkly pigmented African populations ¹⁸. We then applied massively parallel reporter assays (MPRA)¹⁹ to measure the regulatory

activities of 1,157 SNPs residing in open chromatin regions of melanocyte-derived cells and identified 165 variants with significant differential regulatory effects. Using chromosome conformation capture assays and CRISPR-based experiments, we characterized the enhancers and variants regulating the expression of genes related to pigmentation, and demonstrated their impact on melanin levels *in vitro*. Overall, these findings offer valuable insights into the genetic basis of skin pigmentation in African populations.

Results

Identification of candidate regulatory variants impacting skin color

To identify SNPs associated with skin pigmentation in Africa, we first performed genome-wide association studies (GWAS) of skin color using imputed dataset from 1544 eastern and southern African individuals¹³ (GWAS-All, Supplementary Fig. 1, Supplementary Table 1 and Supplementary Note 1) or a subset of 500 individuals from Botswana (GWAS-Bots, Supplementary Fig. 2 and Supplementary Table 2). We further identified SNPs with significant allele frequency differences in the lightly pigmented southern African San compared to other darkly pigmented African populations based on the Di statistic^{18,20} (Di-SNPs, Supplementary Fig. 3 and Supplementary Note 2), which may be enriched for SNPs that are targets of local adaptation and impact the light skin color of the San. To identify variants that may impact enhancer activity, we overlapped the top GWAS-SNPs and Di-SNPs with open chromatin regions from melanocyte-derived cell lines (Fig. 1a and Methods). After filtering, we obtained a total of 1157 SNPs for MPRA, including 340 GWAS-All SNPs, 289 GWAS-Bots SNPs, and 536 Di-SNPs (Fig. 1a).

We applied MPRA to screen for enhancer elements and identify SNPs with variants that show significant differential regulatory activity (Methods, Supplementary Notes. 3 and 4). Specifically, we constructed a MPRA library using synthesized 200-bp oligos centered on each of the two alleles of the 1157 candidate SNPs, along with 150 negative control and 32 positive control oligos (Supplementary Table 3 and Extended Data Fig. 1). We used this library to perform MPRA in two melanoma cell lines: darkly pigmented MNT-1 cells and lightly pigmented WM88 cells (Fig. 1b and Supplementary Figs. 4 and 5). To identify regulatory regions in MNT-1, we conducted CUT&RUN assays using antibodies against H3K4me3, H3K27ac, MITF and SOX10 (Supplementary Fig. 6). We further performed ATAC-seq in both MNT-1 and WM88, and identified 99,718 and 118,486 open chromatin regions, respectively. We found that only 35% of ATAC-seq peaks are shared between these two cell lines (Supplementary Fig. 6b). To decipher the target genes of the candidate SNPs, we constructed a high-resolution chromatin interaction map of MNT-1 cells using Hi-C and H3K27ac HiChIP (Methods, Supplementary Note. 5 and Supplementary Figs. 7–9).

We used “mpralm”²¹ to identify MPRA functional variants (MFVs), which show significant differential regulatory activity between alternative and reference alleles (“allelic skew”). Out of the 1157 tested SNPs, we identified 106 MFVs in MNT-1 and 104 MFVs in WM88, with 45 MFVs shared in both cell lines, for a total of 165 MFVs (Fig. 1c and Supplementary Table 4). Of the 165 MFVs, 77 are Di-SNPs and 88 are GWAS-SNPs (Fig. 1c), indicating that Di analysis and GWAS are complementary methods for identifying potential functional variants related to skin pigmentation. We observed a moderate correlation between the

variant effect sizes in MNT-1 and WM88 ($R = 0.41$, $p = 2.6 \times 10^{-46}$) and 86% of the tested variants showed the same direction of allelic skew (determined by \log_2 -fold change, \log_2FC) in both cell lines (Fig. 1d). Interestingly, rs7948623 (chr11:61137147) near *DDB1* and rs6510760 (chr19:3565253) near *MFSD12* had the largest effect size in MNT-1 and WM88, respectively (Fig. 1e and 1f), suggesting that these two GWAS SNPs may be causal variants at these loci¹³. To validate the allelic skews, we performed luciferase reporter assays (LRA) on 16 MFVs. Among the 16 tested MFVs, 15 MFVs show significant allelic skew in both MPRA and LRA in at least one cell line (MNT-1 or WM88, Supplementary Table 5 and Supplementary Fig. 10). These results indicate that employing two cell lines for the MPRA may enhance the sensitivity for discovering allelic skewed variants that may show differential activity under different *trans*-environments.

***MFSD12* and *HMG20B* are the target genes of rs6510760**

MFSD12 facilitates organellar cysteine transport and impacts melanin levels in melanocytes^{13,22}. MPRA identified six GWAS MFVs (rs6510759, rs734454, rs10416746, rs7246261, rs142317543 and rs6510760) near *MFSD12* that are not in LD with each other ($R^2 < 0.2$; Extended Data Fig. 2 and Supplementary Figs. 11). The previously reported SNP rs112332856, in strong LD with rs6510760 ($R^2 = 0.8$), showed no effect on enhancer activity. Notably, rs6510760 had the largest allelic skew in WM88 ($\log_2FC = 0.6$, $p = 3.4 \times 10^{-32}$) and the sixth most significant allelic skew in MNT-1 ($\log_2FC = 0.51$, $p = 4 \times 10^{-24}$; Supplementary Table 4). *In-silico* analysis revealed that rs6510760 disrupts the binding motif of aryl hydrocarbon receptor (AHR) (Extended Data Fig. 2l), a vital transcription factor involved in melanogenesis²³.

We validated the allelic enhancer activities of four SNPs overlapping regulatory elements upstream of *MFSD12* (rs734454, rs10416746, rs6510760 and rs7246261) using LRA. We found all four SNPs to have significant allelic skew in at least one of the cell lines (Extended Data Fig. 2 and Supplementary Table 5) and all of them are expression quantitative trait loci (eQTLs) of *MFSD12* based on GTEx data (Supplementary Fig. 12). SNPs rs6510760 and rs7246261 in enhancer 4 (E4) are 104 bp apart but not in LD. We explored their combinatorial effects (GC, AC, GT and AT) using LRA. The derived haplotype AT, associated with dark skin color, exhibits reduced enhancer activity compared to the GC haplotype (Supplementary Fig. 13). The results suggests that rs6510760 is the major regulator of enhancer activity, while rs7246261 only has marginal additive effects.

We further applied Hi-C and CRISPR experiments to identify the target genes of rs6510760. Hi-C showed interactions between E4 and the promoters of *MFSD12* and *HMG20B* genes (Extended Data Fig. 3a and 3b, Supplementary Table 6). Compared to controls, CRISPR-inhibition (CRISPRi) of E4 significantly reduced the expression of *MFSD12* and *HMG20B* (Extended Data Fig. 3c–3e), confirming that E4 interacts with both genes. Downregulation of *MFSD12* expression slightly increased melanin levels in MNT-1 (Extended Data Fig. 3f), consistent with previous reports^{13,22}. CRISPR-knockout (CRISPR-KO) of E4 in MNT-1 significantly reduced the expression of *MFSD12* and *HMG20B* (Extended Data Fig. 3g). Together, we validated that rs6510760 is the major regulatory variant affecting the activity

of E4, which impacts the expression of *MFSD12* and *HMG20B* genes and contributes to African skin color variation.

Identification of enhancers and regulatory variants near *OCA2*

OCA2 is the causal gene for oculocutaneous albinism II, which affects human skin, hair, and eye color^{8,13,24–26}. We examined the regulatory activities of 10 Di-SNPs and 16 GWAS-SNPs near *OCA2* using MPRA and identified 4 MFVs (rs4778242 in E1, rs6497271 in E2, rs7495989 in E3, and rs4778141 in E4) (Fig. 2a and Extended Data Fig. 4). These four MFVs showed strong associations with African skin color ($p < 3.4 \times 10^{-5}$, Fig. 2b and Supplementary Fig. 14), but were not in LD ($R^2 < 0.2$, Supplementary Fig. 15) with the previously reported functional SNPs rs12913832¹⁶ and rs1800404¹³. Among these SNPs, rs6497271 showed the greatest allelic skew in both MNT-1 ($p = 8.9 \times 10^{-17}$, Fig. 2c) and WM88 ($p = 3.2 \times 10^{-4}$).

Using Hi-C²⁷ and H3K27ac HiChIP²⁸, we generated a high-resolution (2 kb) chromatin interaction map at the *OCA2/HERC2* locus. We identified a TAD encompassing the *OCA2* promoter and its upstream enhancer regions (Fig. 2d and Supplementary Fig. 16) and detected significant interactions between the promoter and enhancer E2 of *OCA2* by FitHiChIP²⁹ (FDR < 0.05, Supplementary Table 6). CRISPRi of E2 caused a 20% decrease of *OCA2* expression (Fig. 2e), validating the promoter-enhancer interaction. Furthermore, RNA-Seq showed that CRISPRi of E2 had a significant effect on *OCA2* expression ($\log_2FC = -2.76$) but only a marginal effect on *HERC2* expression ($\log_2FC = -0.40$), and it altered the expression of melanogenesis-related genes, such as *DCT*, *PMEL*, and *TYRP1* (Fig. 2f and Supplementary Fig. 17). Notably, CRISPRi of E2 decreased the melanin level in MNT-1 (Fig. 2g). CRISPR-KO of E2 in MNT-1 decreased the expression of *OCA2* and melanin levels by more than 50% (Figs. 2h and 2i, Supplementary Fig. 18). Together, these data highlight the strong effect of E2 on *OCA2* expression.

We further conducted CRISPR/Cas9-mediated genome editing and obtained four clones with SNPs at or next to rs6497271 (Fig. 2j). Notably, all four clones show a significant reduction of *OCA2* expression and melanin levels compared to control (Figs. 2k and 2l). *In-silico* analysis showed that rs6497271 disrupts the binding motifs of SOX10 and LEF1 (Extended Data Fig. 4f), which are key transcription factors in melanocytes. In addition, rs6497271 overlaps a SOX10 binding peak in MNT-1 (Fig. 2a). Thus, the substitution from A to G and the indels at rs6497271 may affect the binding of SOX10, reducing the enhancer activity and subsequent *OCA2* expression. In addition, UKBB GWAS data^{7,30} showed that rs6497271-G is associated with both light skin color and light hair color, indicating that rs6497271 has pleiotropic effects (Supplementary Fig. 19). Collectively, we identified rs6497271 at *OCA2* as a major functional variant affecting human skin pigmentation.

Repeated mutation of an *OCA2* enhancer during human evolution

SNP rs12913832 is a known functional variant associated with blue eye color in Europeans¹⁶ and is 187 bp away from rs6497271. Based on 1000G³¹ and 5M¹³ datasets, the derived allele rs6497271-G is almost fixed (0.984) in Europeans, whereas the ancestral allele rs12913832-A is nearly fixed (0.976) in Africans (Fig. 3a). rs6497271 and rs12913832

form 4 haplotypes (AA, AG, GA, and GG) and we tested the combinatorial effects of these haplotypes using LRA. Haplotype AA showed the highest enhancer activity (75-fold of control in MNT-1); haplotypes AG and GA reduced the enhancer activity to 50–70% of AA; and haplotype GG exhibited the lowest enhancer activity (~25% of AA, Fig. 3b). Consistent with these results, haplotype AA is common in Africans (0.24–0.79) and South Asians (0.16) who have relatively dark skin color; haplotype GA is common in global populations (> 0.21) and has the highest frequency in East Asians (0.98) who have moderately pigmented skin; haplotype GG is at high frequency only in Europeans (0.64) who have light skin color (Figs. 3c and 3d). To determine when these haplotypes formed during human history, we extracted the estimated ages of these two variants from a dataset based on genealogical inference³². The data revealed that the derived allele G at rs6497271 emerged as early as 1.2 million years ago, while the derived allele G at rs12913832 emerged about 57 thousand years ago, coinciding with the migration of modern humans out of Africa (Fig. 3e). These observations suggest that the continuous evolution of the E2 enhancer during human history contributes to current human skin color diversity.

A Di-SNP in *MITF* contributes to light skin color in the San

MITF is a master regulator of melanocyte development and proliferation³³. A cluster of 44 Di-SNPs was identified in the introns of *MITF*, indicating a signature of local adaptation¹⁸ (Fig. 4a and Supplementary Fig. 20). We identified two MFVs: rs111969762 (in E1) and rs7430957 (in E2). Both MFVs are in melanocyte-specific enhancers and colocalize with *MITF* and *SOX10* ChIP-Seq peaks (Fig. 4a and Extended Data Fig. 5a). However, LRA showed that only rs111969762 exhibits regulatory activity, but not rs7430957 (Figs. 4b and 4c, Extended Data Fig. 5d). The discrepancy in enhancer activity for rs7430957 in MPRA and LRA could be due to the difference in enhancer lengths or trans-environment between the two methods³⁴. The enhancer activity of the derived allele rs111969762-T is about 3-fold higher than that of rs111969762-C (Figs. 4b and 4c). In addition, the T-to-C mutation at rs111969762 disrupts the binding motif of FOXP3 (Extended Data Fig. 5e), which is a transcription factor affecting pigmentation³⁵. The ancestral allele rs111969762-C is rare (frequency < 0.05) in most populations but is common in the San (0.47 in Jul'hoansi and 0.63 in !Xoo; Supplementary Fig. 21 and Supplementary Table 7).

Hi-C identified nested TADs at the *MITF* locus and H3K27ac HiChIP detected multiple loops within *MITF* (Fig. 4d and Supplementary Fig. 22). Specifically, we observed a significant interaction (FDR < 0.05 by cLoops³⁶, Supplementary Table 6) between rs111969762 and the TSS of the melanocyte-enriched isoform of *MITF* (*MITF*-M, Fig. 4d). CRISPRi of E1 significantly reduced the expression of *MITF* and melanin levels in MNT-1 (Figs. 4e and 4f), further validating that E1 interacts with the *MITF* promoter by chromatin looping. CRISPR-KO of E1 also significantly reduced the expression of *MITF* and melanin levels in MNT-1 (Figs. 4g and 4h, Supplementary Fig. 23a). RNA-Seq revealed that the E1-knockout affected the expression of genes in melanosome and melanogenesis pathways (Figs. 4i and 4j, and Supplementary Figs. 23b and 23c). For example, we observed downregulation of *DCT*, *MC1R*, *PMEL*, and *SLC24A5*, which are involved in melanogenesis and pigmentation, and upregulation of *LEF1* and *PAX3*, which are upstream transcriptional activators of *MITF*^{37,38}. Collectively, these results indicate that rs111969762

contributes to the relatively light skin color of the San by decreasing the enhancer activity and expression of *MITF*.

The role of Di-SNPs near *LEF1*, *TRPS1* and *BLOC1S6* in pigmentation

We further investigated other regulatory Di-SNPs that could potentially impact skin color in the San. These Di-SNPs include rs11939273 and rs17038630 near *LEF1*; rs75827647, rs10468581, rs113940275 near *NLK*; rs11985280 near *TRPS1* and rs72713175 near *BLOC1S6* (Fig. 5 and Extended Data Figs. 6–9). Based on MPRA and LRA, these Di-SNPs significantly affect enhancer activity in MNT-1 or WM88 (Supplementary Table 5). Among all these SNPs, only rs17038630 near *LEF1*, rs11985280 near *TRPS1*, and rs72713175 near *BLOC1S6* overlap open chromatin regions in MNT-1, WM88 and normal melanocytes (Fig. 5). Importantly, the *LEF1* locus is associated with hair color^{39,40}; the *TRPS1* locus is associated with sunburns³⁹ and tanning⁴¹; and inactivating mutations in *BLOC1S6* cause reduced hair pigmentation in mice⁴². Thus, we further investigated the roles of these loci in pigmentation.

LEF1 is a transcription factor that regulates the expression of *MITF* and *TYR*^{43,44}. Di-SNP rs17038630 is in the third intron of *LEF1* and its derived allele, rs17038630-T, shows higher frequencies in the San (0.80) compared with other populations (< 0.4) (Figs. 5a and 5b). rs17038630-T is associated with decreased enhancer activity compared to rs17038630-G in both MNT-1 and WM88 (Figs. 5c, 5d and Extended Data Fig. 6b), consistent with the observation that the G-to-T mutation at rs17038630 disrupts the binding motif of *LEF1* and *SOX10* (Extended Data Fig. 6c). CRISPRi of enhancer E1 significantly reduced *LEF1* expression and melanin levels in MNT-1 ($p < 0.001$, Figs. 5e and 5f). However, CRISPR-KO of E1 did not significantly impact *LEF1* expression and melanin levels in MNT-1 (Extended Data Fig. 6e). We also identified three functional Di-SNPs near *NLK* by MPRA and LRA (Extended Data Fig. 7 and Supplementary Table. 5). *NLK* is a serine/threonine-protein kinase that phosphorylates *LEF1*^{45,46} and is associated with sunburns³⁹. In summary, we identified regulatory variants near *LEF1* and *NLK*, which may impact pigmentation.

TRPS1 is a transcription factor impacting the development of various tissues, including kidney, bone and hair follicles⁴⁷. We observed that 161 Di-SNPs are located upstream of *TRPS1* and only rs11985280 overlaps a melanocyte-specific ATAC-seq peak (Fig. 5g and Extended Data Fig. 8a). The derived allele rs11985280-C is associated with decreased enhancer activity in both MNT-1 and WM88 (Figs. 5i, 5j and Extended Data Fig. 8b). Consistent with this observation, the T-to-C mutation at rs11985280 disrupts the binding motif of CCAAT/enhancer-binding proteins *CEBPA/B* (Extended Data Fig. 8c). *CEBPA/B* are downstream targets of *STAT3* and loss of *STAT3* enhances pigmentation⁴⁸. CRISPRi of the enhancer containing rs11985280 significantly reduced the expression of *TRPS1* and melanin levels in MNT-1 (Figs. 5k and 5l). CRISPR-KO of the enhancer of *TRPS1* significantly decreased its expression but not the melanin level in MNT-1 (Extended Data Fig. 8d). Based on 180G¹⁸ and SGDP⁴⁹ datasets, the San populations exhibit the highest frequency of rs11985280-C in Africa, with a frequency of 1.00 in Ju|hoansi and 0.97 in !Xoo, followed by the relatively lightly pigmented Ethiopian Amhara population at 0.90. Furthermore, rs11985280-C is nearly fixed in the European (0.997), East Asian (0.997), and

South Asian (0.983) populations based on the 1000G³¹ dataset (Fig. 5h). In comparison, in populations that are relatively more darkly pigmented, including the Baka, Chabu, Dizi, Fulani, Hadza, Herero, Mursi, Sandawe, Tikari and Oceanians, have a lower frequency ranging from 0.17 to 0.43 (Fig. 5h). Indeed, the F_{ST} value for CEU versus YRI (0.714) and CHB versus YRI (0.725) rank in the top 0.05% and 0.1% across the genome, respectively. The GWAS-All dataset shows rs11985280-C is associated with light skin color ($p = 0.088$), although the association is not significant, possibly due to limited power because of lack of variability in the San and Amhara populations. However, the region encompassing *TRPS1* is significantly associated with skin color in the UKBB⁷ dataset (leading SNP rs2721954; $p = 1.2 \times 10^{-91}$). Together, these results suggest that *TRPS1* plays a role in human skin pigmentation in global populations.

BLOC1S6 is involved in intracellular vesicle trafficking and melanosome biogenesis⁵⁰. Using MPRA, we identified a Di-SNP, rs72713175, located 1 kb upstream of *BLOC1S6*, impacting enhancer activity in WM88 (Extended Data Figs. 9a and 9b). The frequency of rs72713175-T, which is correlated with decreased enhancer activity, is much higher in the San (0.61) than in other populations (< 0.31) (Extended Data Fig. 9c). When we tested a 1.8 kb region (including rs72713175 and the promoter of *BLOC1S6*) using luciferase reporter assays, rs72713175 did not significantly affect the enhancer activity in either MNT-1 or WM88, indicating that the effect of rs72713175 on gene expression is negligible relative to the effect of the promoter (Extended Data Fig. 9d). However, CRISPRi of this region significantly reduced *BLOC1S6* expression and pigmentation in MNT-1 (Extended Data Figs. 9e and 9f), suggesting that this SNP lies within a functional enhancer and that *BLOC1S6* impacts pigmentation in human cells, consistent with the observation of decreased pigmentation in a mouse knock-out model.

***TMEM138* and *CYB561A3* are target genes of rs7948623**

Previous studies reported that GWAS-SNP rs7948623 affects the activity of an enhancer interacting with the *DDB1* promoter and hypothesized that *DDB1* may impact skin color variation¹³. In this study, we used MPRA to study 17 GWAS SNPs near *DDB1* and identified 3 MFVs (rs7948623 in E1, rs2277285 in E2 and rs2943806 in E3) in either MNT-1 or WM88 (Fig. 6a and Extended Data Fig. 10). Among the 3 MFVs, rs7948623 had the strongest association with skin color ($p = 1.42 \times 10^{-10}$ in GWAS-All) and showed the most significant allelic skew ($\log_2FC = -2.2$, $p = 2.6 \times 10^{-118}$ in MNT-1; $\log_2FC = -0.2$, $p = 2.3 \times 10^{-7}$ in WM88) as estimated by MPRA and validated by LRA (Fig. 6b and Extended Data Figs. 10b–10d). The ancestral allele rs7948623-A, associated with lighter skin pigmentation, shows higher enhancer activity than the derived allele T (Fig. 6c), indicating that higher activity of E1 is associated with lighter skin pigmentation. Consistently, rs7948623 is located within a MITF binding site in melanocytes and mutation from A to T could disrupt the MITF binding motif (Fig. 6a and Extended Data Fig. 10e). SNPs rs2277285 and rs2943806 are in strong LD with each other ($R^2 = 0.89$) but are in moderate LD with rs7948623 ($R^2 = 0.62$, Extended Data Fig. 10f and 10g). Given that rs7948623 shows the strongest GWAS association and the highest allelic skew, further studies were focused on this SNP.

Using Hi-C and HiChIP, we detected interactions between the E1 enhancer containing rs7948623 and the promoters of *DDB1* (36.5 kb upstream of rs7948623), *CYB561A*, and *TMEM138* (7.8 kb upstream of rs7948623), with the latter two promoters showing stronger interactions (Fig. 6d and Supplementary Fig. 24). CRISPRi or CRISPR-KO of E1 significantly decreased the expression of *TMEM138* and *CYB561A3*, but had only minor effects on *DDB1* expression ($p > 0.1$ for CRISPRi and $p = 0.025$ for CRISPR-KO, Figs. 6e and 6f). RNA-Seq of E1-inhibited MNT-1 confirmed that *TMEM138* and *CYB561A3* show the largest fold-change among all transcribed genes ($\log_2FC = -1.27$ and -1.27 , respectively; Fig. 6g). Similarly, *TMEM138* and *CYB561A3* have the largest differences in gene expression in E1-deleted MNT-1 ($\log_2FC = -0.75$ and -0.84 , respectively; Fig. 6h). *CYB561A3* (Cytochrome B561 Family Member A3) is an ascorbate-dependent ferrireductase in the lysosomal membrane⁵¹ and is highly expressed in skin melanocytes⁵² (TPM = 320, Supplementary Fig. 26). *TMEM138* is a four-transmembrane domain protein involved in ciliary function⁵³ and is moderately expressed in skin melanocytes⁵² (TPM = 37, Supplementary Fig. 26). Collectively, these results suggest that *CYB561A3* and *TMEM138* are the major target genes of rs7948623, and they may play a role in pigmentation.

CYB561A3 affects melanin levels in MNT-1 cells

Although neither CRISPRi nor CRISPR-KO of E1 significantly impacted melanin levels in MNT-1, both of them significantly affected the expression of known genes related to melanosome and melanogenesis pathways (Figs. 6i and 6j and Supplementary Fig. 25). Considering that deletion of E1 significantly reduces expression levels of *CYB561A3* and *TMEM138* (Figs. 6f and 6h) and that the allele at rs7948623 with higher enhancer activity is associated with lighter skin pigmentation (Figs. 6b and 6c), we hypothesized that decreasing the expression of *CYB561A3*/*TMEM138* may enhance pigmentation. Indeed, overexpression of either *CYB561A3* or *TMEM138* in MNT-1 significantly reduced melanin levels *in vitro* (Fig. 7a and Supplementary Fig. 27), while the negative control CD63-GFP had no significant effects. Importantly, overexpression of *CYB561A3* had a considerably larger impact on melanin levels compared to *TMEM138* ($\log_2FC = -2.2$ versus -0.34 , Fig. 7a) and did not affect cell proliferation in MNT-1 (Supplementary Fig. 27c).

To understand how *CYB561A3* could regulate pigmentation, we investigated its sub-cellular localization using confocal imaging of immunostained HA-tagged human *CYB561A3*. In HeLa cells, *CYB561A3*-HA co-localized with the lysosomal protein LAMP1 (Supplementary Fig. 27d), as previously reported⁵¹. In MNT-1, however, a significant fraction of *CYB561A3*-HA ($79.45\% \pm 2.85\%$) co-localized with TYRP1 protein found primarily in mature melanosomes (Figs. 7b and 7c), suggesting that *CYB561A3* might regulate pigmentation.

To investigate the transcriptome-wide effects of *CYB561A3*, we performed RNA-Seq of MNT-1 exogenously expressing *CYB561A3* (Fig. 7d). Overexpression of *CYB561A3* affects the expression of genes involved in mitochondrial respiration and melanin production (Figs. 7e and 7f, and Supplementary Fig. 28). Notably, the gene most strongly downregulated in MNT-1 overexpressing *CYB561A3* was *DCT* ($\log_2FC = -1.1$, $p =$

1.1×10^{-21} , DESeq2, Figs. 7d and 7f), which encodes an enzyme critical for melanin biosynthesis. In addition, other genes that directly or indirectly regulate melanosome function, including *MC1R*, *PMEL*, and *SLC45A2*, were also downregulated (Fig. 7f). Moreover, increased *CYB561A3* expression also decreased the expression levels of genes related to mitochondrial function (Fig. 7f).

Similar to the deletion of the E1 enhancer of *CYB561A3* (Fig. 6), partial *CYB561A3*-knockout (69%) had no significant effect on melanin levels in MNT-1, likely due to the already high levels of melanin in these cells (Supplementary Figs. 25c and 29). However, RNA-Seq of these CRISPR-modified cells showed that decreased *CYB561A3* significantly altered the expression of genes related to melanosome in MNT-1 (Figs. 7g–i and Supplementary Fig. 30), consistent with the effects of E1-deletion described above (Fig. 6j and Supplementary Fig. 25e). For example, *SLC24A5* and *TYR*, which positively regulate melanin production^{54–56}, were upregulated; whereas *MFSD12* and *TPCN2*, which negatively regulate melanin production^{13,57}, were downregulated in cells with reduced *CYB561A3* mRNA. Taken together, we identified *CYB561A3* as a novel negative regulator of skin pigmentation.

Discussion

The San populations from Botswana have relatively light skin color compared to other African populations^{5,13}, possibly due to local adaptation, but the underlying genetic mechanism remains to be uncovered. We identified 77 Di-SNPs that are MFVs that alter enhancer activities in melanocyte-derived cells and validated the function of regulatory Di-SNPs near *MITF*, *LEF1*, *TRPS1* and *BLOC1S6* using LRA and CRISPR-based experiments. *MITF*, *LEF1* and *TRPS1* play important roles in the Wnt signaling pathway^{45,46,58–61}, regulating the development of melanocytes and hair^{62,63}. Given that the San have relatively light skin color and a unique hair morphology compared to other African populations^{18,64}, these Di-SNPs may not only contribute to the light skin color of the San but also play a role in their hair phenotypes. These results shed light on the genetics and evolutionary history of light skin color in the San population.

Most of the GWAS-SNPs and Di-SNPs (> 98%) are located in noncoding regions, and SNPs in noncoding cis-regulatory elements could impact the expression of several genes, making it more difficult to directly determine the leading causal variants and their target genes⁶⁵. Indeed, we discovered that the enhancer harboring rs6510760 affects the expression of *MFSD12* and *HMG20B*, both of which may impact pigmentation phenotypes; the enhancer harboring rs6497271 regulates the transcription of *OCA2* and *HERC2*; the enhancer harboring rs7948623 affects the expression of *CYB561A3* and *TMEM138*, with a smaller effect on *DDI1*. These results revealed that one variant could affect multiple genes and, thus, have pleiotropic effects.

Human skin color variation is likely determined by hundreds of loci^{4–13,66,67}. Inclusion of ethnically diverse and underrepresented populations in future genetic studies will be informative for identifying more loci underlying human skin pigmentation, as well as other variable phenotypes. In addition, since the causal variants/genes at most GWAS

loci have not been confirmed, there is an urgent need for experimental validation. MPRA and CRISPR-based screens are promising high-throughput methods for transforming associations into causations, which will broaden our knowledge of complex traits and the treatment of human diseases.

Methods

Samples and ethics

The collection of samples and data for this study conformed to all relevant ethical regulations. Before sample collection, we obtained permits from local institutions in Africa. An appropriate IRB (Institutional Review Board) approval was also obtained from the University of Pennsylvania. All individuals involved in this study have approved written informed consents. For the details of the sample information of the 5M array data, see Crawford et al.¹³. For the details of sample information of the 180 WGS data, see Fan et al.¹⁸. The melanin index data was inferred using red reflectance values from skin in a minimally sun-exposed region (underside of the arm), as detailed in Crawford et al.¹³.

Cell lines and cell culture

MNT-1 (ATCC, #CRL- 3450), a gift from Dr. Michael S. Marks at Children's Hospital of Philadelphia Research Institute, were grown in DMEM (Gibco, #11965084) supplemented with 20% Fetal Bovine Serum (FBS), 1% GlutaMAX (Gibco, #35050061), 1% NEAA (Gibco, #10370021), 1% penicillin/streptomycin (Gibco, #15140122), and 10% AIM-V (Gibco, # 12055-091).

WM88 (Rockland, #WM88-01-0001), a melanocytic patient-derived melanoma tumor cell line, a gift from Dr. Ashani Weeraratna at Wistar Institute, was cultured in Tumor Specialized medium (80% MCDB153, 20% Leibovitz's L-15, supplemented with 2% fetal bovine serum (FBS) and 1.68 mM CaCl₂).

HeLa cells (CCL-2, ATCC) were cultured in DMEM supplemented with 10% FBS and 100 units/mL penicillin/streptomycin. Lenti-X 293T cells (Takara, # 632180) were cultured in DMEM (Gibco, #11965084) supplemented with 10% FBS and 1% penicillin/streptomycin (Gibco, #15140122). All cells were cultured at 37°C with 5% CO₂ in a humidified incubator.

Genome-wide association analysis

We conducted a genome-wide association analysis of skin color variation using 32,574,188 SNPs imputed from a previously published Illumina 5M SNP array dataset¹³ of 1544 African samples originating from Ethiopia, Tanzania, and Botswana (GWAS-All). The SNPs were imputed using the following reference datasets: the 180 WGS¹⁸ data was merged with SGDP⁴⁹ samples. Briefly, we imputed the 5M array data¹³ using Minimac3 and excluded SNPs with low quality (genotype quality score < 0.3) and low frequency (MAF < 0.00001 in the pooled dataset). The GWAS was conducted using a linear mixed model (EMMAX⁷³) implemented in EPACKS⁷⁴ (Efficient and Parallelizable Association Container Toolbox, v3.3.0), and using kinship, sex, age, and top 10 PCs as covariates. We

also performed a GWAS for 505 individuals from Botswana (GWAS-Bots, which includes 314 San individuals, and is a subset of the GWAS-All dataset) using the same software and parameters. The script used is: `epacts single -vcf [input.vcf.gz] --ped [input.ped] --min-maf 0.01 --kinf [input.kinf] --pheno [PHENO_NAME] --cov [COV1] --cov [COV2] --out [outprefix] --run [# of parallel jobs] --test q.emmax --anno`. The association results were ranked based on p-values and the top 4999 SNPs were selected for downstream functional analysis.

Di analysis

To identify highly differentiated SNPs between the relatively lightly pigmented San population (Ju|'hoan and !Xoo) and other African populations, we calculated the D_i values for 9,413,188 variants from our 180G dataset (12 populations, 15 samples per population, Fan et al. ¹⁸) and selected SNPs with the top 0.1% d_i values for downstream functional analysis as described in Fan et al. ¹⁸. The D_i statistic is calculated using the following equation:

$$D_i = \sum_{j \neq i} (F_{ST}(i, j) - E[F_{ST}(i, j)]) / sd(F_{ST}(i, j))$$

where $F_{ST}(i, j)$ is the F_{ST} value at a SNP site between population i and j , $E[F_{ST}(i, j)]$ and $sd[F_{ST}(i, j)]$ is the mean and standard deviation of F_{ST} values. F_{ST} measures the proportion of the genetic variance contained in a subpopulation relative to the genetic variance in all populations. Values range from 0 to 1, with higher values indicating greater genetic differentiation between populations ⁷⁵. We performed 3 D_i analyses: Ju|'hoan and !Xoo vs other populations; Ju|'hoan vs other populations (excluding the !Xoo); !Xoo vs other populations (excluding the Ju|'hoan). SNP enrichment analyses were conducted using GREAT (V4.04) ⁷⁶ and FUMA (V1.5.4) ⁷⁷. GREAT and FUMA calculate statistics by associating SNPs with their two nearest genes and use the genes as input for enrichment analysis.

SNP filtering and selection

We selected GWAS SNPs for the massively parallel reporter assay located within melanocyte open chromatin regions (ATAC-Seq/DNase-Seq peaks from melanoma cells and melanocytes) using the following 18 datasets from the ENCODE ⁶⁸ and GEO ⁷⁸ databases: GSM2476338, GSM2476339, GSM2476340, GSM2575295, GSM3083210, GSM774243, GSM1024610, GSM774244, GSM816631, GSM1027307, GSM1027312, GSM1014535, GSM1024793, GSM1024779, ENCF560LQG, ENCF600JNF, ENCF862XVF, GSM1008599. We used GNU Wget v1.21.3 to download data from ENCODE. To select D_i -SNPs related to skin pigmentation, we overlapped the top 0.1% D_i -SNPs with melanocyte open chromatin regions as described above. We then focused on the D_i -SNPs located within 1Mb distance to the TSS of 760 candidate pigmentation related genes. The 760 pigmentation-related genes were manually collected from 3 sources: 107 genes associated with pigmentation phenotype in mice (<https://www.mousephenotype.org/data/phenotypes/MP:0001186>) ⁷⁹; 650 genes from a published review ⁸⁰; top 100 genes highly expressed in the SK-MEL-30 cell line based on the protein atlas database ⁸¹.

Luciferase reporter assay

The MNT-1 and WM88 cell lines were used for luciferase reporter assays. The cells were plated in 24-well plates at 0.1M per well, and 500 ng firefly luciferase plasmid, 20 ng pRL Renilla luciferase plasmid (Promega, # E2231) and 1.5 μ L Lipofectamine 3000 (Invitrogen, #L3000150) were added to each well. 36 hours post-transfection, luciferase activity was determined using Dual-Luciferase Assay kit (Promega, # E1910) according to manufacturer instructions. The luminescence signal was detected in a white 96-well plate using a SpectraMax i3x Multi-Mode Microplate Reader. The reporter gene activity of firefly luciferase was normalized to that of Renilla luciferase to determine the activity of functional elements.

Plasmid cloning

For luciferase assay, human enhancer elements were cloned using genomic DNA extracted from MNT-1. The amplified enhancer fragments were sequenced and ligated to PGL4.23 vector (Promega, #E8411) using Gibson assembly (NEB, #E2621). Candidate functional SNPs were introduced by mutated primers. For CRISPR inhibition experiments, sgRNAs were designed at IDT (https://www.idtdna.com/site/order/designtool/index/CRISPR_CUSTOM) or CRISPOR (<http://crispor.tefor.net/>) and cloned into pLKO5.sgRNA.EFS.GFP (Addgene, #57822) backbone vector using BsmBI. For CYB561A3 and TMEM138 cloning and expression, pL-CRISPR.EFS.GFP (Addgene, #57818) plasmid was digested using BamH1 and Nhe1, and the 7.5kb fragment was gel extracted as the vector backbone. Human CYB561A3 and TMEM138 CDS were PCR amplified using cDNA from MNT-1. The CDS and vector (7.5kb) fragments were assembled by Gibson assembly and transformed into Stb13 competent cells. Plasmids were extracted using NucleoSpin Transfection-grade Kit (Takara, #740490.250) and sequenced to confirm the plasmid sequence. Oligo sequences are listed in the supplementary table.

CRISPR knockout and inhibition

To perform enhancer CRISPR knockout or inhibition, we first constructed MNT-1 stable-expressing Cas9 (lentiCRISPR v2, Addgene, #52961) or dCas9-KRAB-MeCP2 (Addgene, #110821). Then, we produced lentiCRISPR v2 (KO) and dCas9-KRAB-MeCP2 (CRISPRi) lentiviruses following the published protocol¹⁹. Then, MNT-1 were infected with each virus with 8 μ g/mL Polybrene (Sigma CatNo.H9268). For KO cell line, 24hrs post infection, medium was replaced using full medium with Puromycin (2 μ g/mL, Gibco, #A1113803), medium was changed every 24 hours. After selection for 5 days, the MNT-1 were passaged to a 10cm plate. The MNT-1-Cas9 cells were frozen for CRISPR-KO experiments. For CRISPRi cell line, all procedures are similar except that the cells were selected with Blasticidin (5 μ g/mL, Gibco, #A1113903).

For CRISPR knockout of the enhancers, MNT-1 stable-expressing Cas9 were seeded in 24-well plates at a density of 0.05M per well and cultured for 24 hours. Then the medium was changed to fresh medium with 8 μ g/mL Polybrene before infection. PLKO5-sgRNA (target to enhancer) viruses were added at ~10 MOI, plates were centrifuged at 1000g for 30min at 32 °C. 24 hours post infection, medium was replaced using full medium with

Puromycin (2 µg/mL), and changed every 24hrs. 5 days after infection, the cells were harvested for total RNA extraction or melanin assay.

For enhancer CRISPR inhibition, MNT-1 stably expressing dCas9-KRAB-Mecp2 cells were seeded in 24-well plates at a density of 0.05M per well and cultured for 24 hours. The medium was changed to fresh medium with 8 µg/mL Polybrene (MNT-1) before infection. PLKO5-sgRNA virus were added at ~10 MOI, plates were centrifuged at 1000g for 30min at 32 °C. 24 hours post infection, medium was replaced using full medium with Blasticidin (5 µg/mL) and was changed every 24 hrs. 5 days after infection. Finally, the cells were harvested for RNA extraction or melanin assay.

RT-qPCR and RNA-Seq

Total RNA was purified from all the cultured cells (CRISPR KO, CRISPR inhibition, Overexpression) using Direct-zol RNA Miniprep Kits (Zymo, R2052) following manufacturer's instructions, and concentration was determined by a Nanodrop. For RT-qPCR, 200–500 ng RNA was used for reverse transcription using M-MLV Reverse Transcriptase (Promega, # M1701) and Random Primer Mix (NEB, S1330). qPCR was conducted using Luna Universal qPCR Master Mix (NEB, M3003) on a QuantStudio 6 Flex Real-Time PCR machine (see primers in Supplementary Table 8). For RNA-Seq, a total of 500 ng RNA was sent to Genewiz to prepare sequencing libraries (see details at <https://web.genewiz.com/rna-seq-faq>). Briefly, mRNA was selected by Poly(A) enrichment, followed by fragmentation and reverse transcription, and addition of sequencing adapters and amplification. The final library was sequenced on HiSeq 2000 (150bp PE) at a depth of 20 million reads per library.

Immunostaining

Human CYB561A3 in pCMV-C-HA (Sino Biological, HG16893-CY) was transiently expressed in MNT-1 or HeLa cells using TransIT-LT1 Transfection Reagent (Mirus Bio) according to the manufacturers' instructions. Transfected cells on glass coverslips were fixed with 4% paraformaldehyde at room temperature for 15 min. Cells were incubated with 50 mM NH₄Cl for 10 min to quench free aldehyde groups, followed by incubation with blocking solution (0.2% saponin, 0.1% BSA, 0.02% sodium azide) containing primary antibodies for 1 hr at room temperature. Following 4 × 5 min PBS washes, coverslips were incubated in fluorescently labeled secondary antibodies in blocking solution for 1 hr at room temperature. Coverslips were washed with PBS for 5 mins (4 times) and inverted onto slides with ProLong Diamond Antifade Mountant. Antibodies used were mouse anti-TYRP1 (TA99/mel-5, 1:100, BioLegend), mouse anti-LAMP2 (H4A3, 1:20, Developmental Studies Hybridoma Bank), and rat anti-HA (ROAHAHA, 1:50, Roche). Host-specific secondary antibodies were conjugated to AlexaFluor 488 or 568 and used at a dilution of 1:1000.

Confocal microscopy and image analysis

Images were acquired using an Olympus FV3000 laser scanning confocal microscope with a 60x objective (1.3 NA; UPlan Super Apochromat). Colocalization analysis was performed using CellSens Dimension (v. 3.2). Briefly, each multichannel image was converted into an 8-bit image with a single channel. A region of interest (ROI) > 10% of the cell surface

area with low organelle density was selected for analysis. We generated binary images using the multiply channels operation, composite images were generated of two channels, where the total fluorescence of composite images was divided by the fluorescence of each single channel to calculate the percent overlap between channels.

Melanin assay

MNT-1 cells were washed with PBS twice and detached with 0.25% trypsin. The cells were pelleted at 300 g for 3 mins at room temperature, and the supernatant was removed gently. The cell pellet was washed once with PBS and lysed in 200 μ L lysis buffer (50 mM Tris-HCl, pH 7.4, 2 mM EDTA, 150 mM NaCl, 1 mM dithiothreitol) per million cells. The lysis was vortex 3 times, every 5 minutes and then spanned down at 12,000 g for 10 mins at 4°C. 50 μ L supernatant was saved for protein quantification (BCA assay, Thermo Scientific, #23225). Then, 150 μ L 2X Protease Lysis buffer (20 mM Tris (pH 8), 200 mM NaCl, 50 mM EDTA, 1% SDS, 0.5 mg/mL proteinase K) was added to the rest lysate to digest the pellet. Pellets were rotated at 65 °C for 5 hours and span down at 12,000g for 10 min to collect melanin. The melanin pellets were dissolved in 0.45 mL buffer N (2M NaOH/ 20% DMSO) and incubated at 60°C for 30 mins with shaking. Once melanin has fully dissolved (or if not, sonicated for 5 mins). The melanin concentration was measured by absorbance at 450 nm. If necessary, the melanin was diluted so that the absorbance value is less than 0.35.

MPRA

We performed MPRA following the lentiMPRA¹⁹ protocol with minor modifications, see details in Supplementary Notes. 3 and 4. The data analysis workflow was illustrated in Supplementary Fig. 4. Specifically, The paired-end 150bp reads (R1 and R3) covering the 200bp enhancer fragments were merged using Flash⁸² (-m 50 -M 92). We obtained 98.6 million merged reads of which 46.1% had the expected 200bp length, 30.1% were 1 bp short, and 11.7% were 2 bp short (short reads were excluded from downstream analysis). We extracted the 15bp barcodes (R2) associated with each merged read and filtered out low-quality read pairs. At this step, we had 29.3M high-quality read pairs (R1_ R3_ R2). We aligned the merged sequences to the reference enhancer sequences using BWA (bwa mem -t 4 -L 50 -k 10 -O 6 -B 5). To construct a unique enhancer-barcode dictionary, we removed repeated enhancer-barcode pairs and low-frequency pairs (< 3 read pairs). We also filter the pairs using the SAM-CIGAR string (\$3=="200M" && \$4=="MD:Z:200") to remove errors introduced by synthesizing and/or sequencing. The average barcode types per oligo is 126, and the average barcode count per oligo is 4284 in the pre-library (Asso_Lib). In this library, there are 1102 reference alleles, 1103 alternative alleles, 148 negative controls, and 30 positive controls. We sequenced the barcodes using pair-end 15bp reads (r1 and r3) and merged them using Flash⁸² (-m 15 -M 15). We filtered out low-quality read pairs (r1_r3_r2) using fastp⁸³ and removed PCR duplicates based on UMI. At this step, we have 66%–74% reads remaining for barcode counting. We matched and counted the barcodes in the DNA and RNA libraries based on the enhancer-barcode associated library. Around 32% of the barcodes in the DNA and RNA libraries could be found in the association library. We detected 1099 Ref-Alt pairs (SNPs) in the DNA and RNA libraries. After obtaining the raw barcode counts from the DNA and RNA libraries, we performed allele-specific effect (ASE) analysis using the R package "mpra"²¹. We prepared KxS integer matrices (K is barcode

count, S is sample) and constructed a MPRASet object for both DNA and RNA libraries. We applied weighted linear models to test for differential enhancer activity using mpralm (normalize = TRUE, model_type = "corr_groups").

RNA-Seq analysis

Raw RNA-Seq fastq files were retrieved from Genewiz server, and read quality was checked using FastQC (<https://github.com/s-andrews/FastQC>). Low-quality reads and adapters were filtered out using fastp⁸³ with default settings. Reference transcriptome (refMrna.fa.gz, hg38) and gene annotation (refGene.txt.gz, hg38) was downloaded from UCSC database. Transcript abundance was quantified by kallisto⁸⁴ with default settings. Gene level read counts were calculated using Tximport package⁸⁵ and genes with mean read count less than 10 were discarded. Differential expression genes were identified using DESeq2⁸⁶ and DEBrowser⁸⁷. Differential expressed genes with adjusted p-value or unadjusted p-value less than 0.05 were selected for volcano plot using EnhancedVolcano⁸⁸ package. Pathway enrichment analysis was performed using Pathview⁸⁹.

ATAC-Seq

MNT-1 or WM88 cells were washed with PBS twice and detached with 0.25% trypsin. The cells were pelleted at 500g for 5 mins at 4°C and the cell density was quantified by an Automated Cell Counter. Then, 50,000 viable cells were used for ATAC-seq following the Omni-ATAC protocol⁹⁰. Tn5 tagmentase was purchased from Diagenode (Cat. No. C01070010).

Each ATAC-seq library was sequenced at a depth of > 40 M pair-end reads by Nextseq 550. Then, the raw fastq files were filtered using fastp (v 0.22.0)⁸³ with default settings and mapped using bowtie2 (v 2.4.1)⁹¹ with parameters "--very-sensitive --maxins 1000". Duplicates and low-quality reads were removed using MarkDuplicates from gatk⁹² (v 4.1.7.0) and samtools (v 1.13)⁹³ with parameters "-q 20 -F 1804 -f 2". Bam files were converted to Bigwig files using deeptools2 (v 3.1.3)⁹⁴ with the setting "--normalizeUsing RPKM --binSize 10". ATAC-seq peaks were called using macs2 (v 2.1.0.20150731)⁹⁵ with the setting "callpeak -t in.bam -g hs -f BAMPE -q 0.01 --keep-dup all". The fraction of reads in peaks were calculated using featureCounts (v 2.0.3)⁹⁶. TSS enrichment plots and correlation analysis were conducted using deeptools2⁹⁴.

CUT&RUN

MNT-1 cells were washed with PBS twice and detached with 0.25% trypsin. The cells were pelleted at 500g for 5 mins at 4°C and then fixed with 0.1% formaldehyde at room temperature for 1.5 min. Then, cells were quenched by adding 2.5 M glycine solution to a final concentration of 0.2 M. Finally, 500,000 cells were used for CUT&RUN using the CUT&RUN Kit (Cat. No. 14–1048) from epicypher. The antibodies used for CUT&RUN include: MITF (CST, #97800), SOX10 (CST, #89356), and H3K27Ac (abcam, # ab4729). H3K4me3 and IgG antibodies were from the CUT&RUN kit. All procedures were conducted following the manufacturer's manual.

Each CUT&RUN library was sequenced at a depth of > 8 M pair-end reads by Nextseq 550. First, H3K4me3 antibody specificity was determined using the SNAP-CUTANA K-MetStat Panel. Second, the raw fastq files were filtered using fastp (v 0.22.0)⁸³ with default settings and mapped using bowtie2 (v 2.4.1)⁹¹ with parameters “--dovetail --very-sensitive-local -I 10 -X 700”. Duplicates and low-quality reads were removed using MarkDuplicates from gatk⁹² (v 4.1.7.0) and samtools (v 1.13)⁹³ with parameters “-q 20 -F 1804 -f 2”. Bam files were converted to Bedgraph and normalized using scale factors determined by spike-in Ecoli reads. Bam files were also converted to Bigwig files using deeptools2 (v 3.1.3)⁹⁴ with the setting “--normalizeUsing RPKM --binSize 10”. H3K27ac CUT&RUN peaks were called using macs2 (v 2.1.0.20150731)⁹⁵ with the setting “callpeak -t in.bam -g hs --broad --broad-cutoff 0.05 -f BAMPE --keep-dup all”. MITF, SOX10 and H3K4me3 CUT&RUN peaks were called using SEACR (v 1.3)⁹⁷. The fraction of reads in peaks was calculated using featureCounts (v 2.0.3)⁹⁶. TSS enrichment and correlation were conducted using deeptools2⁹⁴.

Transcription factor binding analysis

We used “motifbreakR”⁶⁹ (v2.14.2) to predict the potential transcription factor binding motifs near functional SNPs. Briefly, we first transformed the SNP id to Granges using the “snps.from.rsid” function. Then, we used motifs from the hocomoco database⁹⁸ to predict effects for candidate variants. We visualize the candidate broken motifs using the plotMB function.

Identification of SNP-Gene pairs by TAD and loops

To identify the SNPs and their potential target genes in the same TAD, we intersected the SNPs with all TADs called by onTAD⁷¹ from all Hi-C experiments (see details in supplementary notes). Then, we intersected the TADs with transcription start sites (TSS) from all human genes. We paired SNPs and genes that are in the same TAD. To identify the SNPs and their potential target genes by Hi-C or H3K27ac HiChIP loops, we extended the SNPs and TSSs to 2kb fragments (SNP/TSS \pm 1kb). Then, we intersected the anchors of loops with these 2kb bins and paired the SNPs and TSSs located in the anchors of the same loop.

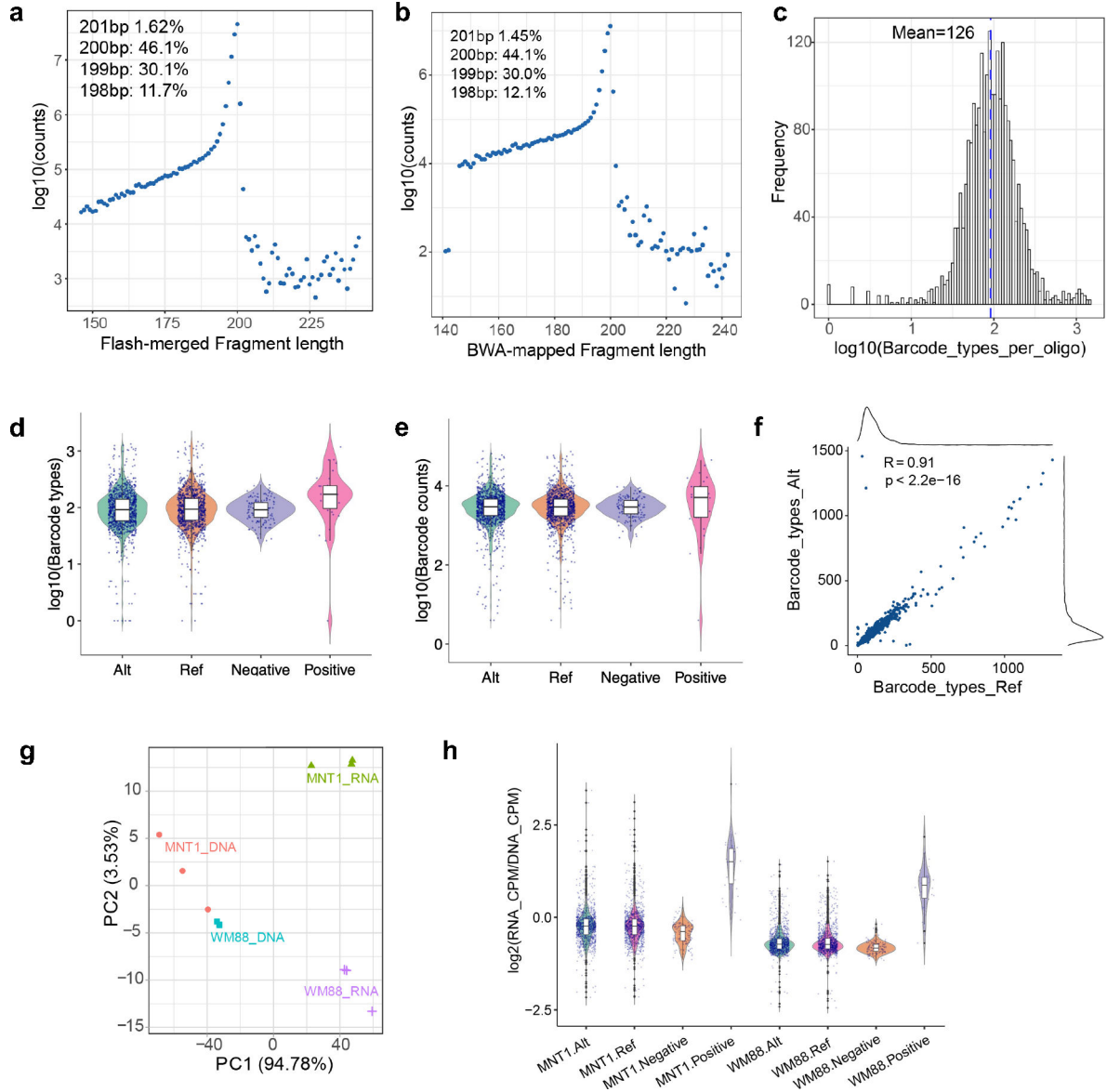
Statistics and reproducibility

No statistical method was used to determine the sample size in advance. No data were excluded from the analyses. We randomly selected controls for MPRA. For confocal images and related quantification of MNT-1 cells, the cells were randomly selected. Other experiments were not randomized. The investigators were not blinded to allocation during the experiments and outcome assessment.

Additionally, the two-sided paired t-test is utilized to compare the means of two groups in luciferase reporter assays. Two-sided unpaired t-test is applied to compare the means of two groups with unpaired data, specifically in CRISPRi and CRISPR-KO assays. When comparing the means among more than two groups, we initially conducted a one-way ANOVA. Subsequently, we performed the two-sided Tukey’s test with adjustments for multiple comparisons or the two-sided Dunnett’s test with adjustments for multiple

comparisons (with control group). In the case of MPRA, the p-values were estimated using a random effects model for mpralm²¹, and paired t-tests were conducted with multiple testing adjustments.

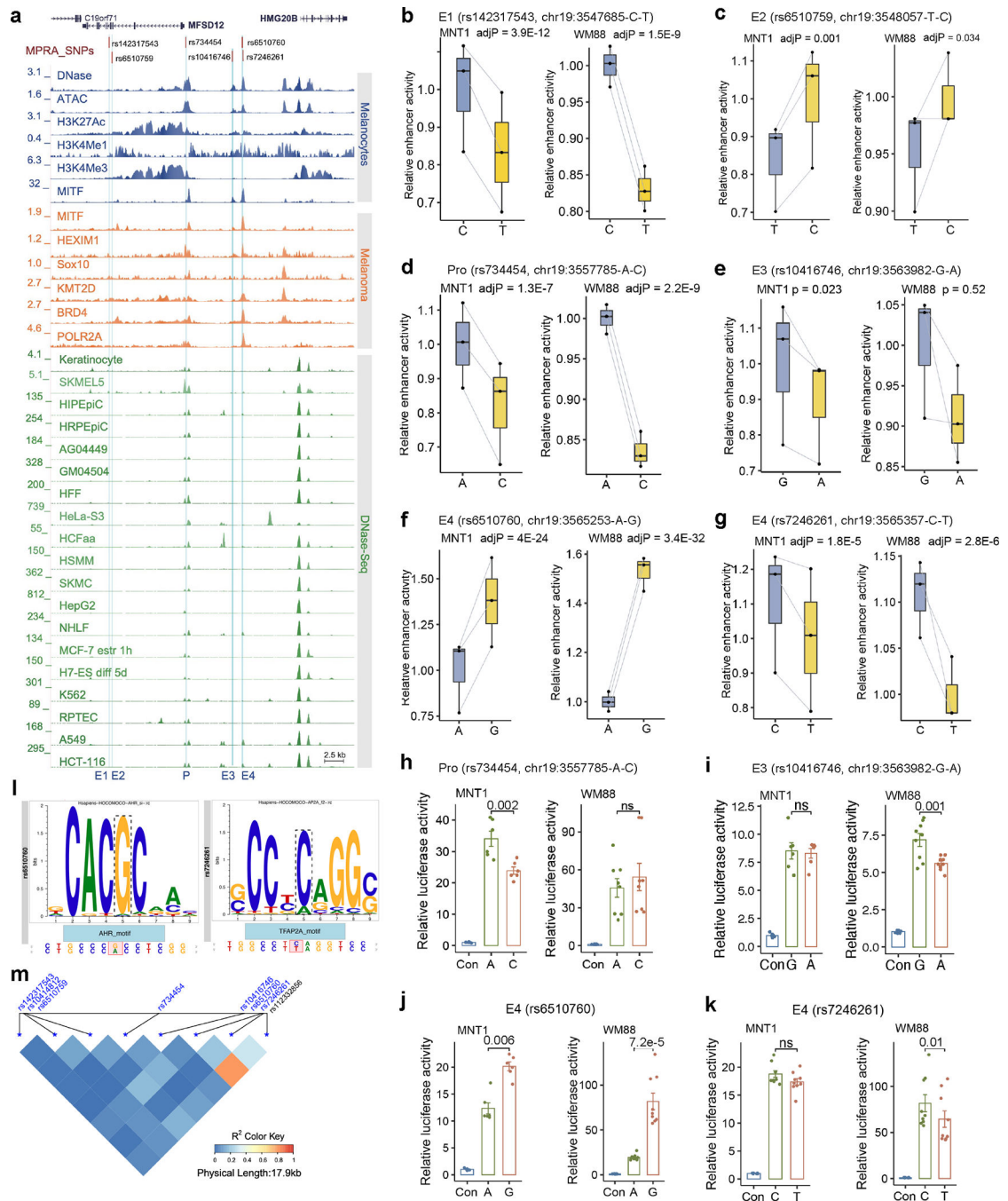
Extended Data



Extended Data Fig. 1. Quality statistics of the MPRA experiments.

(a) Statistics for FLASH-merged reads in the association library. The plot showed that 46.1% are 200bp fragments as designed. (b) Statistics of BWA-mapped reads in the association library. The plot showed that 44.1% are 200bp fragments as designed. (c) Statistics of barcode types per oligo in the association library. On average, each oligo is linked with 126 different barcodes. (d) Statistics of barcode types per oligo in reference (n = 1102), alternative (n = 1103), negative control (n = 153), and positive control (n = 30)

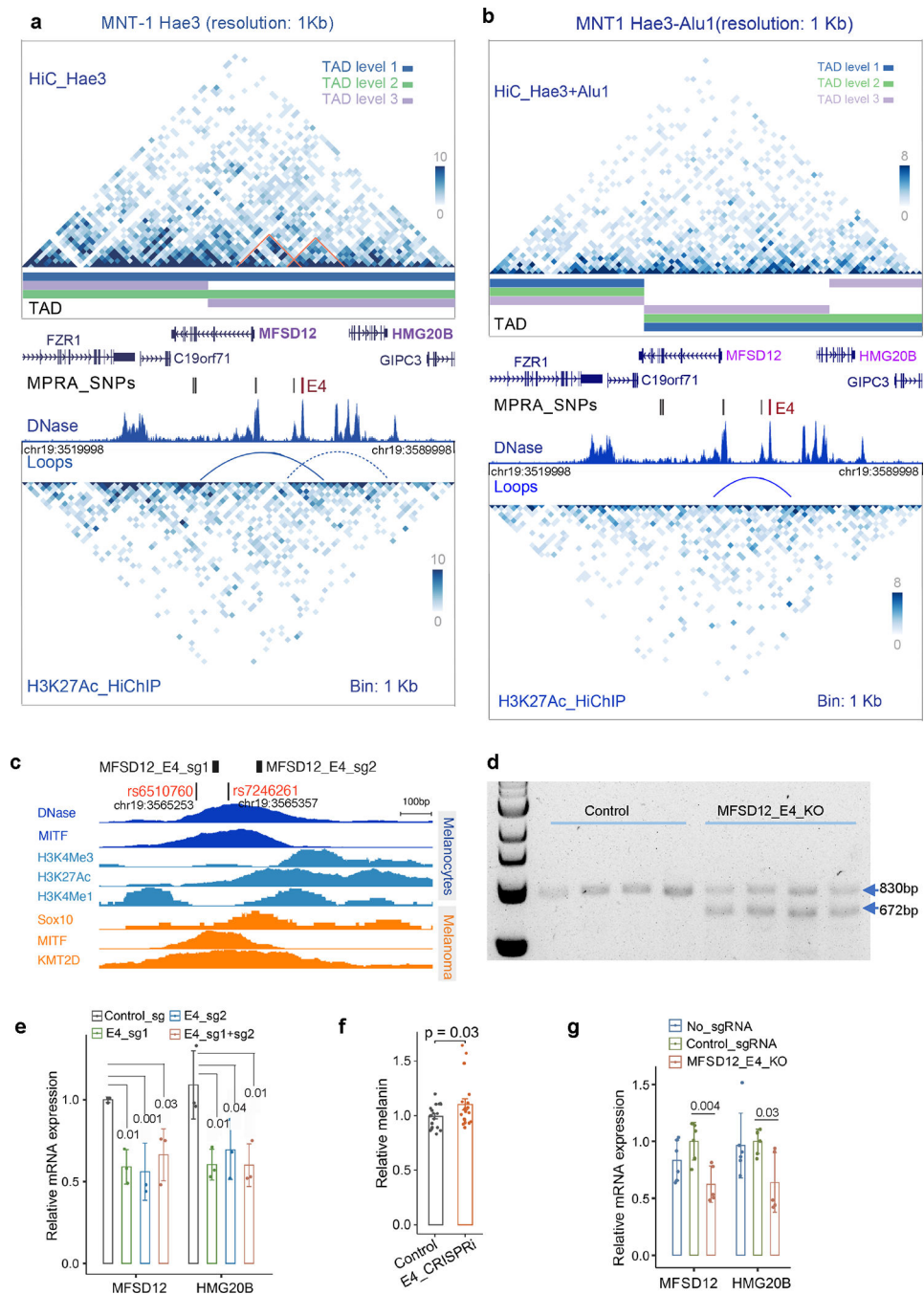
oligos. Data is from the association library. **(e)** Statistics of barcode counts per oligo in reference (n = 1102), alternative (n = 1103), negative control (n = 153), and positive control (n = 30) oligos. Data is from the association library. **(f)** Barcode types for reference and alternative alleles are comparable. Pearson's $r = 0.91$, $p < 2 \times 10^{-16}$. **(g)** Principal component analysis of DNA and RNA libraries from MNT-1 and WM88 cells. Three replicates. **(h)** Summary of enhancer activities estimated by MPRA. Enhancer activities were defined as the barcode counts per million in the RNA library divided by the barcode counts per million in the DNA library. Alt: oligos containing alternative alleles (n = 1103). Ref: oligos containing reference alleles (n = 1102). Negative, negative control oligos (n = 148). Positive, positive control oligos (n = 30). For boxplots, central lines are median, with boxes extending from the 25th to the 75th percentiles. Whiskers further extend by ± 1.5 times the interquartile range from the limits of each box.



Extended Data Fig. 2. MPRA identifies six allelic skewed variants near *MFSD12*.

(a) Plot showing allelic skewed variants in regulatory regions near *MFSD12*. Blue tracks show DNase-Seq, ATAC-Seq, and ChIP-Seq data from melanocytes; orange tracks indicate ChIP-Seq data from melanoma (501-mel) cells, green tracks indicate DNase-Seq data from ENCODE cell lines. E1-E4, enhancers. P, promoter. (b-g) Relative enhancer activities of the two alleles at rs142317543, rs6510759, rs734454, rs10416746, rs6510760, rs7246261 estimated by MPRA (n = 3). For b, c, d, f, g, p-values were estimated with a random effects model for mpralm and paired t-tests with multiple testing adjustments; e was without

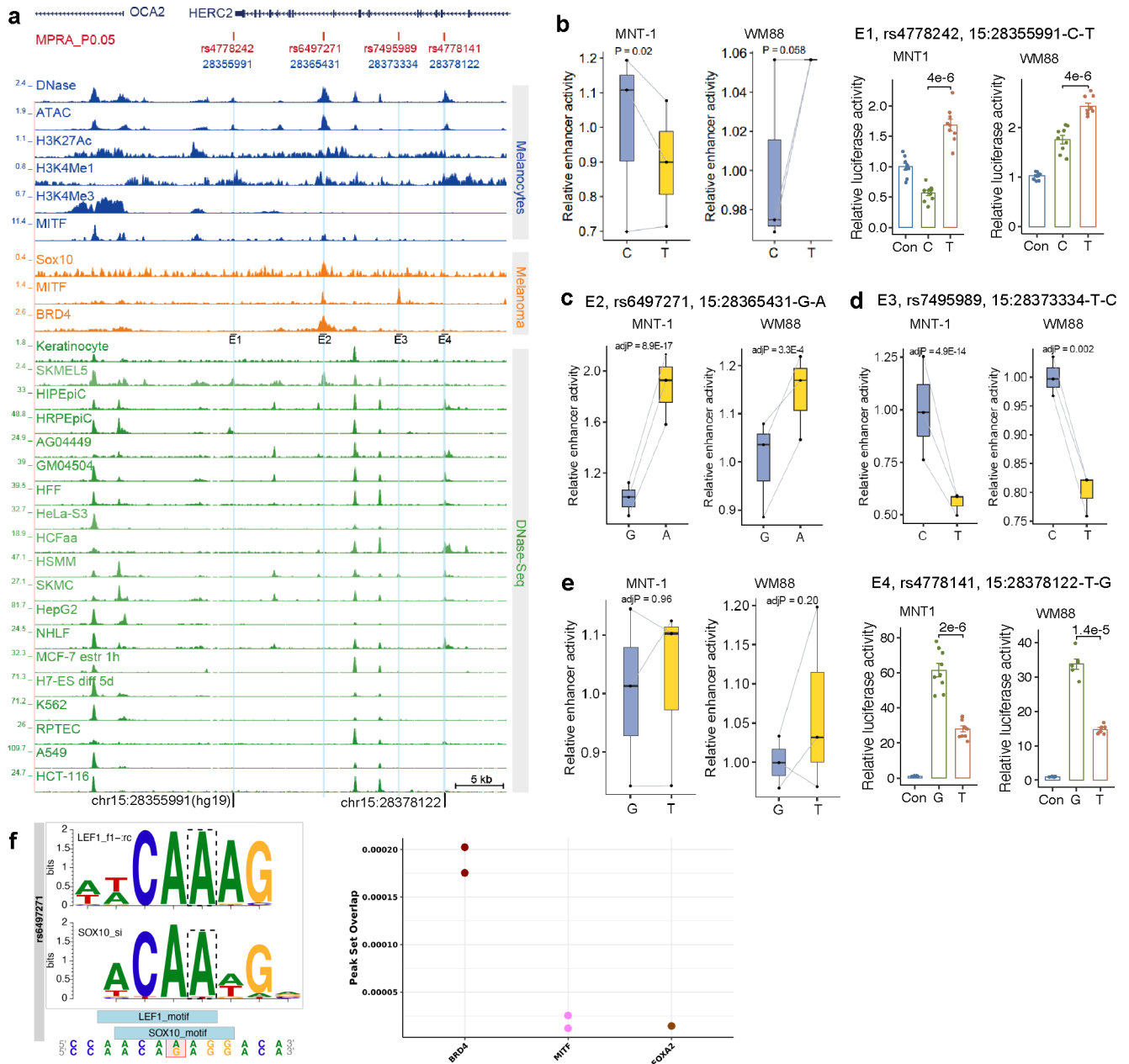
multiple testing adjustments. **(h-k)** Relative enhancer activities estimated by LRA. Two-tailed paired t-tests (For LRA in MNT1, n=6. For LRA in WM88, 2h n=8; others n=9). Data were presented as mean \pm SEM. ns $p > 0.05$. **(l)** rs6510760 and rs7246261 disrupt the binding motifs of AHR and TFAP2, respectively. Predicted by “MotifBreakR”⁶⁹. **(m)** The LD pattern of candidate functional variants near *MFS12*. LD was calculated using the 180G¹⁸ data by the LDheatmap⁷⁰ package. For boxplots, central lines are median, with boxes extending from the 25th to the 75th percentiles. Whiskers further extend by ± 1.5 times the interquartile range from the limits of each box.



Extended Data Fig. 3. The enhancer E4 interacts with the promoter of *MFSD12* and affects the expression of *MFSD12*.

(a-b) Chromatin interactions near *MFSD12* identified by Hi-C and H3K27ac HiChIP with Hae3 digestion. The upper matrix is from MNT-1 Hi-C data, and the lower matrix is from MNT-1 H3K27ac HiChIP data. TADs were called by onTAD⁷¹ and colored by nested TAD levels. The solid arch was a loop defined using FitHiChIP²⁹ software, the dashed arch was a potential loop based on the observed interaction matrix. The interaction matrix between *MFSD12* and *HMG20B* were highlighted with orange angles. The DNase track of melanocytes was downloaded from ENCODE⁶⁸. rs6510760 and rs657246261 in E4

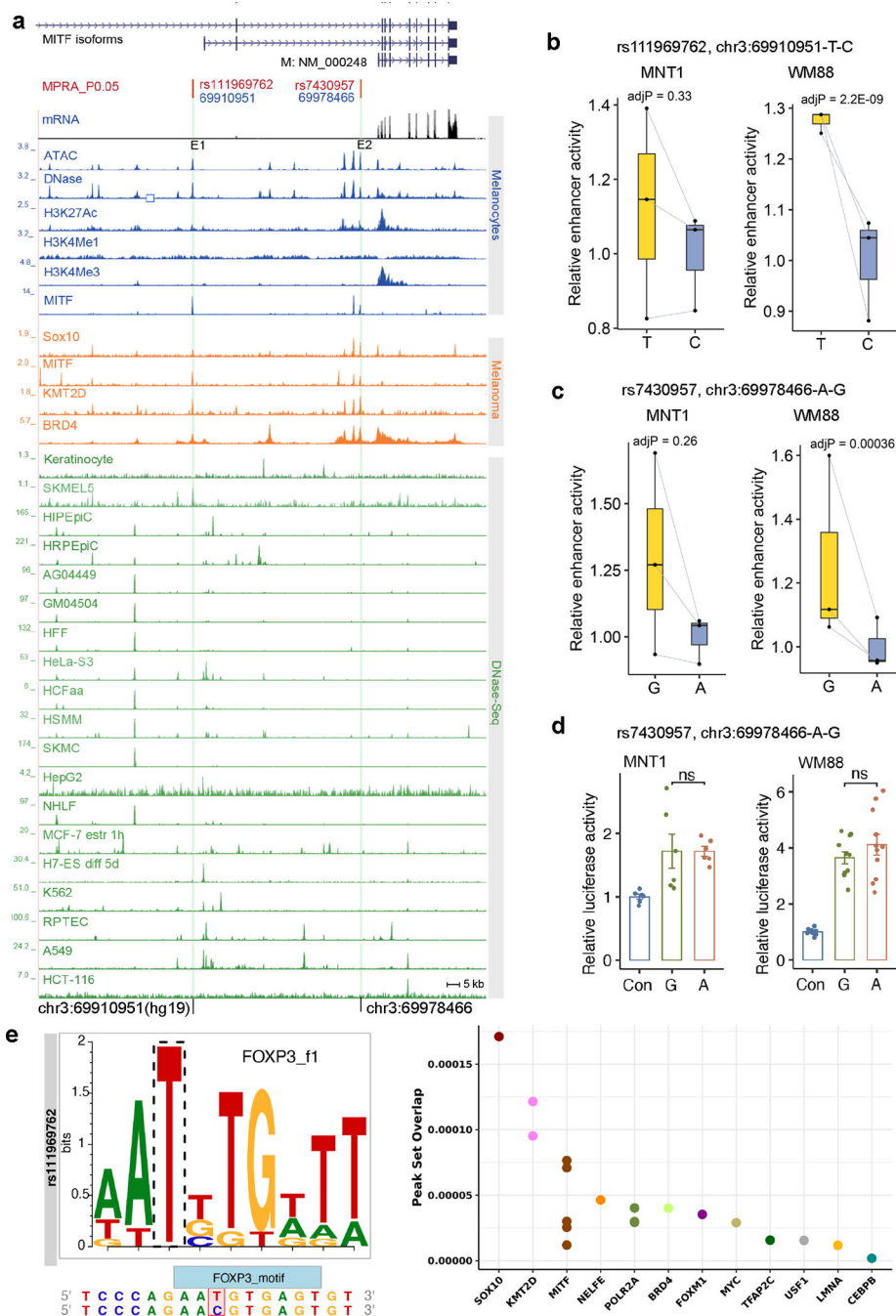
are colored in red. The plotted region is chr19:3519998–3589998 (hg19). (c) Schematic showing the location of the two sgRNAs targeting the enhancer E4 of *MFSD12*. (d) PCR results showing efficient knockout of the enhancer by the two sgRNAs. Three independent experiments. (e) qPCR showed that CRISPRi of E4 significantly decreases the gene expression of *MFSD12* and *HMG20B* in MNT-1 cells. Two-sided Dunnett's test with adjustments for multiple comparisons (n = 3). (f) CRISPRi of E4 significantly increases melanin levels in MNT-1 cells. Two-tailed unpaired t-tests (n = 19). (g) qPCR showed that CRISPR knockout of E4 significantly decreases the gene expression of *MFSD12* and *HMG20B* in MNT-1 cells. Two-tailed unpaired t-tests without multiple testing adjustments (n = 6). Data are presented as mean ± SEM.



Extended Data Fig. 4. Identification of functional variants associated with skin pigmentation near *OCA2*.

(a) SNP rs6497271 is in a melanocyte-specific enhancer. Blue tracks indicate DNase-Seq, ATAC-Seq, and ChIP-Seq data from melanocytes; orange tracks indicate ChIP-Seq data from melanoma (501-mel) cells; green tracks indicate DNase-Seq data from ENCODE cell lines. E1-E4, enhancers. The plotted region is chr15: 28,335,146–28,385,146 (hg19). (b) MPRA and LRA revealed that rs4778242 significantly affects the enhancer activity of E1 in MNT-1 and WM88. MPRA (n = 3), LRA (n = 9). (c) MPRA showed that rs6497271 significantly affects the enhancer activity of E2 in MNT-1 and WM88 cells (n = 3). (d) MPRA showed that rs7495989 affects the enhancer activity of E3 in MNT-1 and WM88 cells (n = 3). (e) MPRA and LRA revealed that rs4778141 affects the enhancer activity

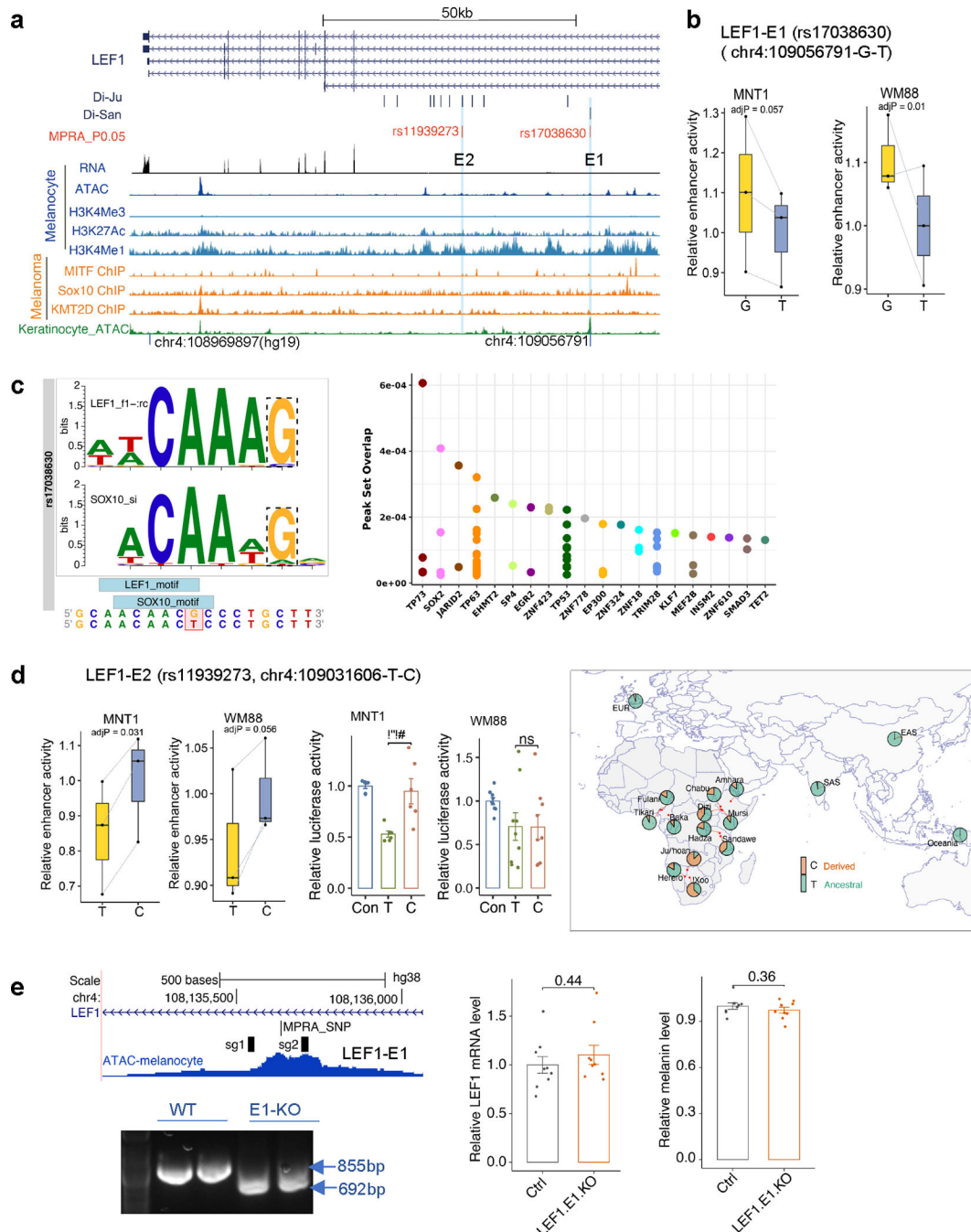
of E4 in MNT-1 and WM88 cells. MPRA ($n = 3$), LRA (MNT-1, $n = 9$; WM88, $n = 6$). (f) rs6497271 overlaps transcription factor binding sites. Left panel showed rs6497271 disrupts the binding motif of LEF1 and SOX10. Right panel showed the rs6497271 overlaps CHIP-seq peaks from Cistrome database⁷². LRA data are presented as mean \pm SEM, tested with two-tailed paired t-tests. MPRA p-values were estimated with a random effects model for mpralm and paired t-tests with multiple testing adjustments. For MPRA boxplots, central lines are median, with boxes extending from the 25th to the 75th percentiles. Whiskers further extend by ± 1.5 times the interquartile range from the limits of each box.



Extended Data Fig. 5. Identification of functional variants near *MITF* related to skin pigmentation in the San.

(a) A plot showing that functional Di-SNP rs111969762 is in a melanocyte-specific regulatory region. Blue tracks show DNase-Seq, ATAC-Seq, and ChIP-Seq data from melanocytes; orange tracks indicate ChIP-Seq data from melanoma (501-mel) cells, green tracks indicate DNase-Seq data from ENCODE⁶⁸. E1-E2, enhancers. (b) MPRA showed that rs111969762 affects enhancer activity in WM88 cells (n = 3). (c) MPRA showed that rs7430957 impacts enhancer activity in WM88 cells (n = 3). (d) LRA showed that

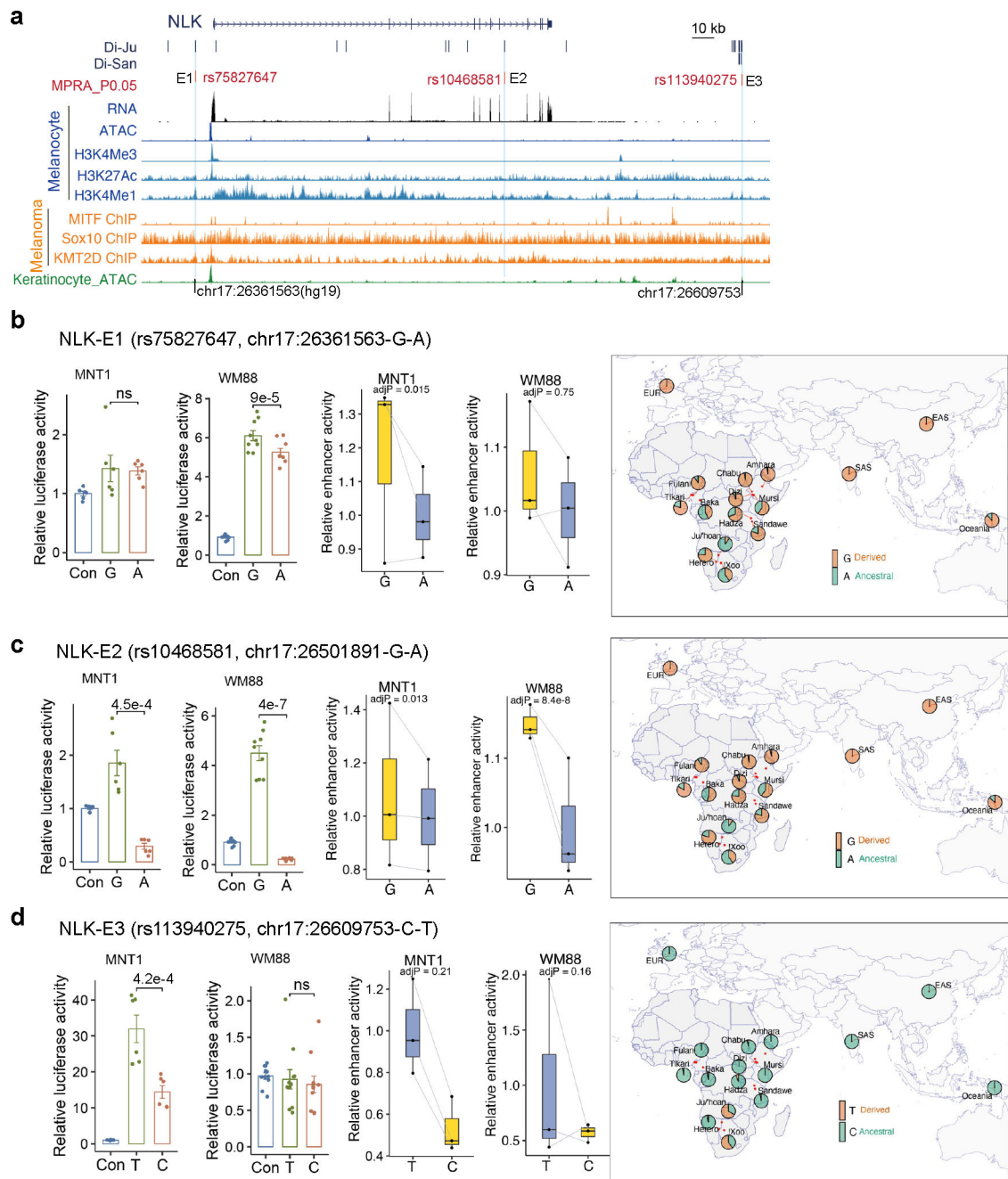
rs7430957 does not significantly alter the activity of the E2 enhancer near *MITF*. P values were estimated by two-tailed paired t-tests, MNT-1 (n = 6), WM88 (n = 11). Data were presented as mean \pm SEM. ns p > 0.05. (e) rs111969762 overlaps transcription factor binding sites. Left panel shows that rs6497271 disrupts the binding motif of FOXP3. Right panel shows that rs111969762 overlaps ChIP-seq peaks from the Cistrome database⁷². MPRA p-values were estimated with a random effects model for mpralm and paired t-tests with multiple testing adjustments. For MPRA boxplots, central lines are median, with boxes extending from the 25th to the 75th percentiles. Whiskers further extend by ± 1.5 times the interquartile range from the limits of each box.



Extended Data Fig. 6. Functional testing of Di-SNPs near *LEF1*.

(a) MFVs and regulatory elements near *LEF1*. rs17038630 and rs11939273 are Di-SNPs from the San population. (b) Plot showing allelic skews at rs17038630 in MNT-1 and WM88 cells estimated by MPRA (n = 3). (c) rs17038630 overlaps SOX10 and LEF1 binding sites. Left panel shows that rs17038630 disrupts the binding motif of SOX10 and LEF1. Right panel shows that rs11939273 overlaps ChIP-seq peaks from the Cistrome database⁷². (d) MPRA and LRA results showing allelic skews at Di-SNP rs11939273 in MNT-1 and WM88 cells, the allele frequency data was from the 180G¹⁸ and 1000G

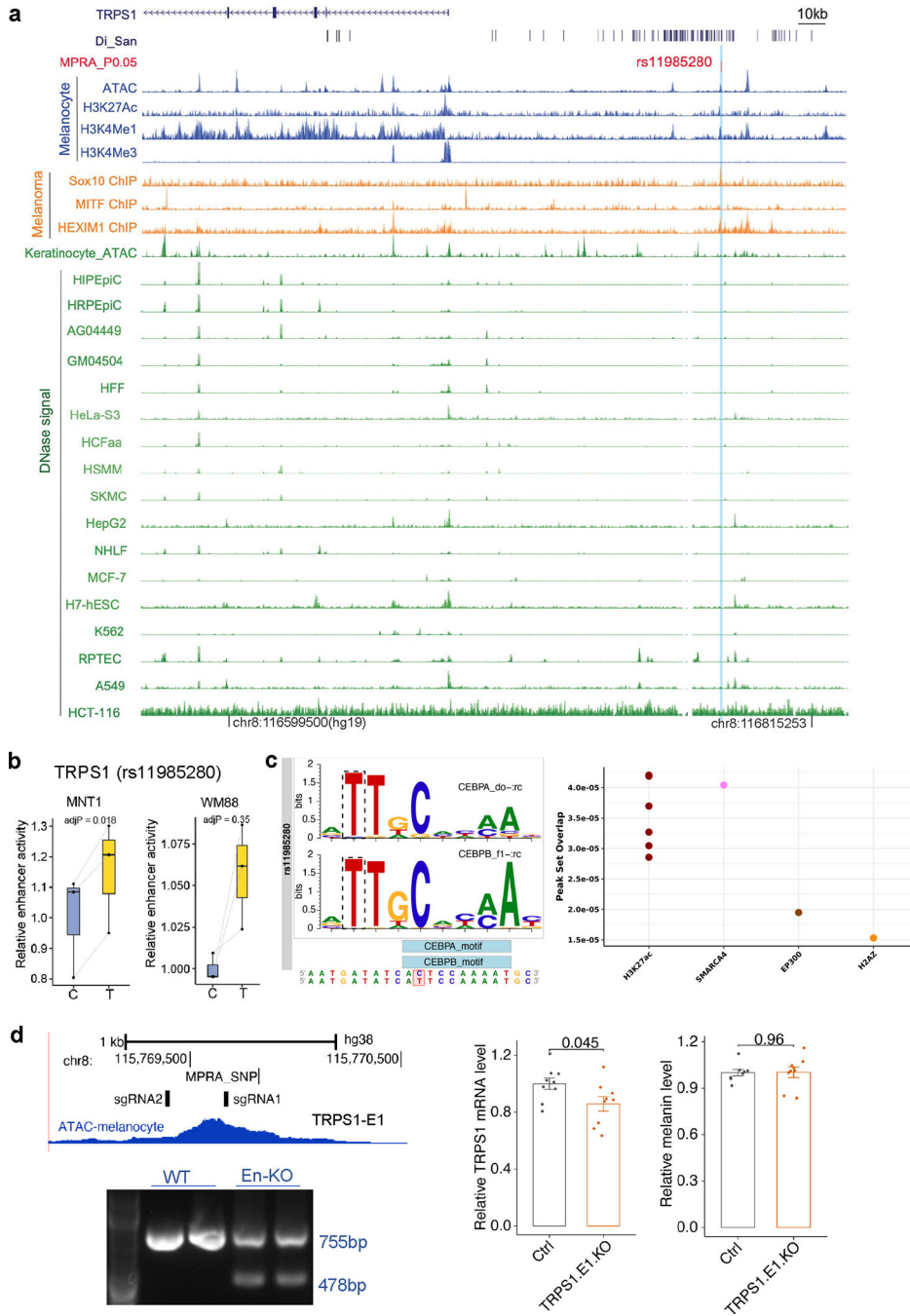
³¹datasets. LRA data are presented as mean \pm SEM, tested with two-tailed paired t-tests, MPRA (n = 3), LRA (MNT-1, n = 6; WM88, n = 9). (e) CRISPR-KO of the enhancer E1 of *LEF1* does not affect LEF1 expression and melanin levels in MNT-1 cells. Left panel shows genotyping results of CRISPR-KO of the enhancer E1 of *LEF1*, three independent experiments. Middle panel shows the RT-qPCR results of CRISPR-KO of the enhancer E1 of *LEF1* (n = 9). Right panel shows the melanin levels of CRISPR-KO of the enhancer E1 of *LEF1* (n = 9). Two-tailed unpaired t-tests. For MPRA boxplots in b and d, central lines are median, with boxes extending from the 25th to the 75th percentiles. Whiskers further extend by ± 1.5 times the interquartile range from the limits of each box. MPRA p-values were estimated with a random effects model for mpralm and paired t-tests with multiple testing adjustments.



Extended Data Fig. 7. MPRA and LRA identified three functional Di-SNPs near *NLK*.

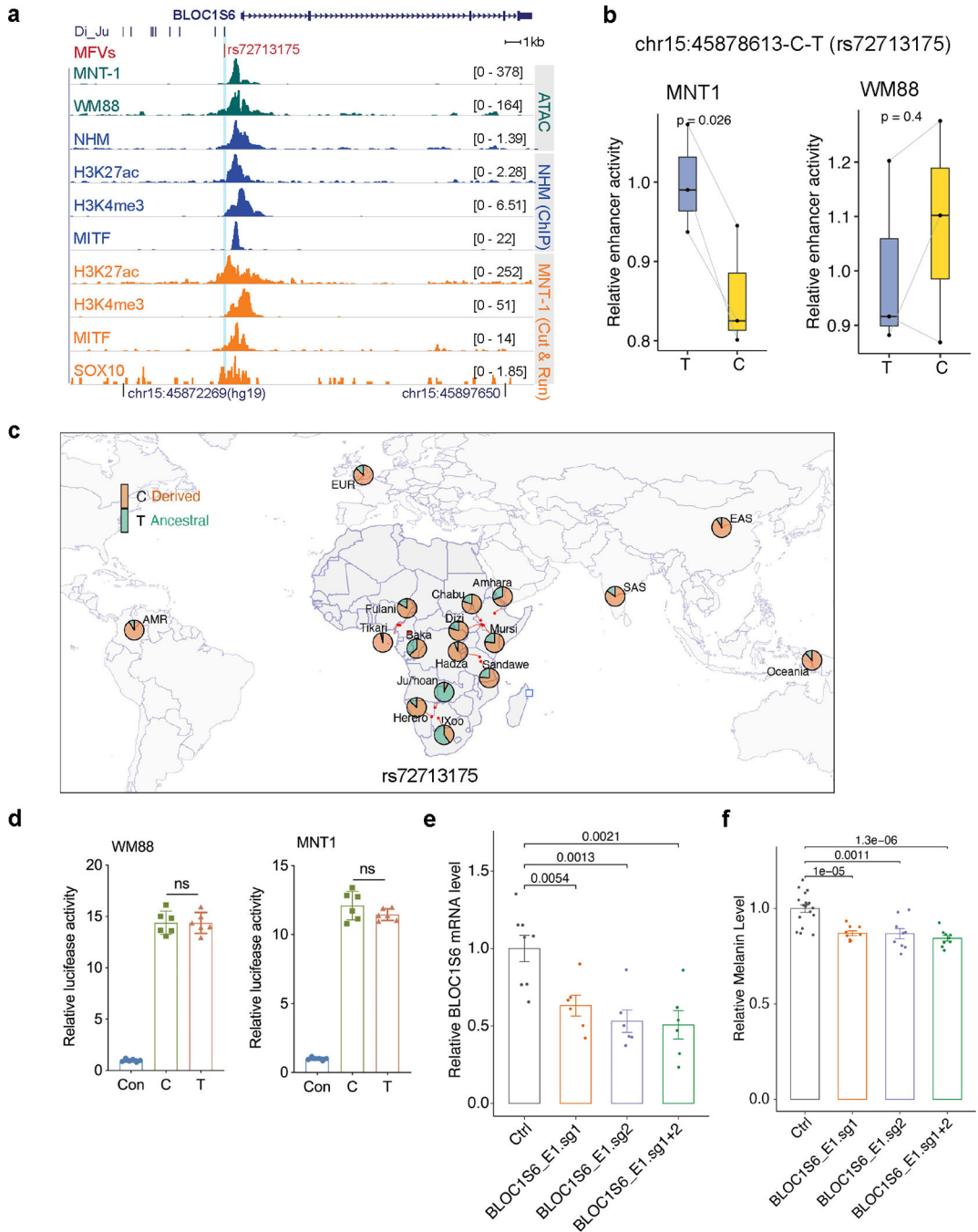
(a) MFVs and regulatory elements near *NLK*. rs75827647, rs10468581 and rs113940275 are Di-SNPs from the San population. (b) LRA and MPRA results showing allelic skews at rs75827647 in MNT-1 and WM88 cells. MPRA (n = 3), LRA (MNT-1, n = 6; WM88, n = 9). (c) LRA and MPRA results showing allelic skews at rs10468581 in MNT-1 and WM88 cells. MPRA (n = 3), LRA (MNT-1, n = 6; WM88, n = 9). (d) LRA and MPRA results showing allelic skews at rs113940275 in MNT-1 and WM88 cells. MPRA (n = 3), LRA (MNT-1, n = 6; WM88, n = 11). From b to d, the barplots are results of LRA. Two-tailed paired t-tests without adjustments for multiple comparisons, data were presented as mean \pm

SEM. ns $p > 0.05$. The boxplots are results from the MPRA, p -values were estimated with a random effects model for mpralm and paired t-tests with multiple testing adjustments. The right panels are allele frequency maps constructed using the 1000G¹⁸ and 1000G³¹ datasets. For boxplots, central lines are median values, with boxes extending from the 25th to the 75th percentiles. Whiskers further extend by ± 1.5 times the interquartile range from the limits of each box.



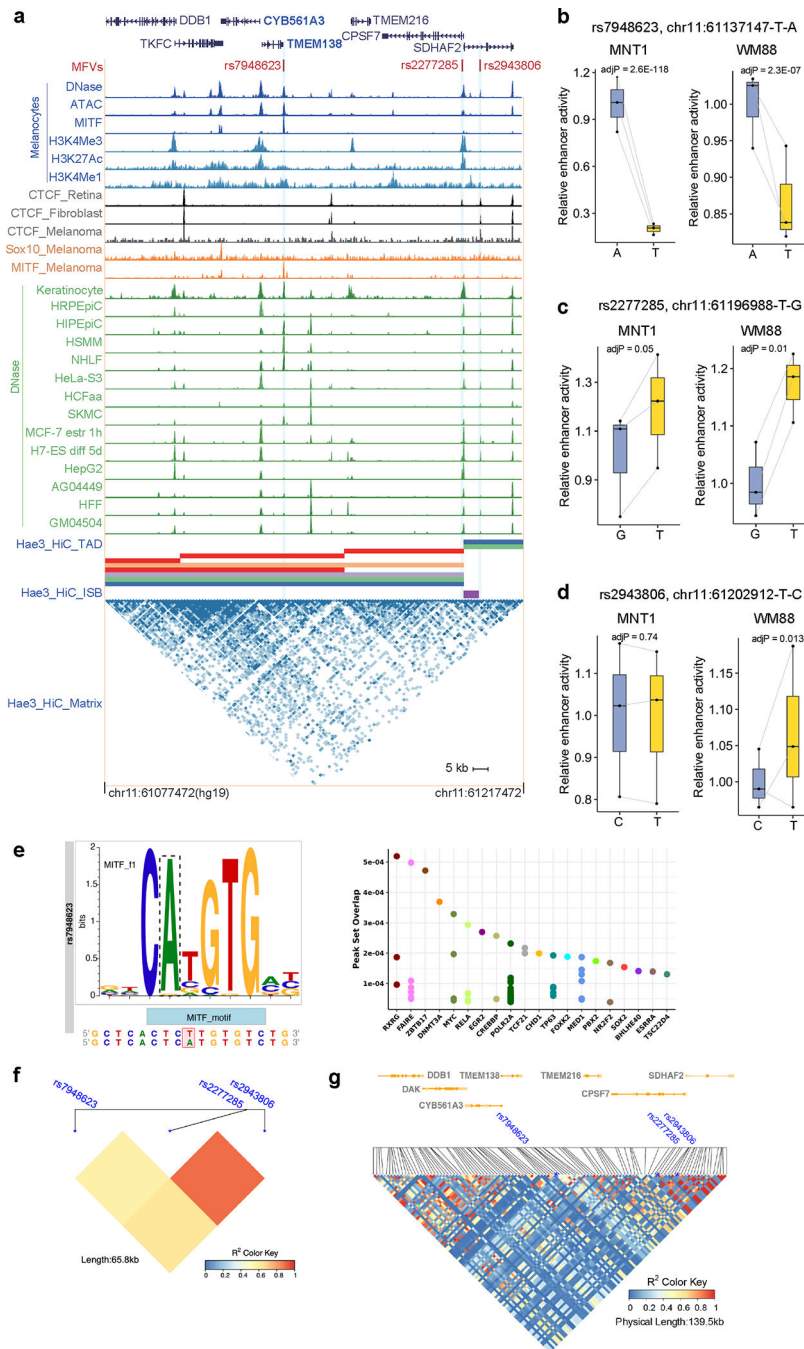
Extended Data Fig. 8. Functional testing of Di-SNPs near *TRPS1*.

(a) SNP rs11985280 overlaps a regulatory element of *TPRS1*. Blue tracks show ATAC-Seq, and ChIP-Seq data from melanocytes; orange tracks indicate ChIP-Seq data from melanoma (501-mel) cells, green tracks indicate ATAC-Seq and DNase-Seq data from ENCODE⁶⁸. (b) MPRA results showing allelic skews at rs11985280 in MNT-1 and WM88 cells (n = 3). p-values were estimated with a random effects model for mpralm and paired t-tests with multiple testing adjustments. For boxplots, central lines are median, with boxes extending from the 25th to the 75th percentiles. Whiskers further extend by ± 1.5 times the interquartile range from the limits of each box. (c) rs11985280 disrupts the binding motif of CEBPA and CEBPB. Right panel shows that rs11985280 overlaps ChIP-seq peaks from the Cistrome database⁷². (d) CRISPR-KO of the enhancer E1 of *TRPS1* affects *TRPS1* expression but not melanin levels in MNT-1 cells. Left panel shows genotyping results of CRISPR-KO of the enhancer E1 of *TRPS1*, three independent experiments. Middle panel shows the RT-qPCR results of CRISPR-KO of the enhancer E1 of *TRPS1* (n = 9). Right panel shows the melanin levels of CRISPR-KO of the enhancer E1 of *TRPS1* in MNT-1 cells (n = 9). Two-tailed unpaired t-tests. Data were presented as mean \pm SEM and p values were listed above the bars.



Extended Data Fig. 9. Identification of functional regulatory variants near the *BLOC1S6* locus. (a). rs72713175 overlaps a regulatory region in melanocytes. Green tracks represent ATAC-seq for MNT-1 and WM88 cells; blue tracks show ATAC-Seq and ChIP-Seq data from normal human melanocytes (NHM); orange tracks indicate CUT&RUN data from MNT-1 cells. (b) MPRA results showing allelic skews at rs11985280 in WM88 cells but not in MNT-1 cells (n = 3). P values were estimated with a random effects model for mpralm and paired t-tests without multiple testing adjustments. For boxplots, central lines are median, with boxes extending from the 25th to the 75th percentiles. Whiskers further extend by

± 1.5 times the interquartile range from the limits of each box. (c) Allele frequencies at rs72713175 in global populations, data were from the 180G¹⁸ and 1000G³¹ datasets. (d) LRA results showing that rs72713175 did not affect enhancer activity in WM88 and MNT-1 cells. Two-tailed paired t-tests (n = 6). (e) CRISPRi of the enhancer containing rs72713175 significantly reduced the expression of *BLOC1S6* (control, n = 8; others, n = 6; Two-sided Dunnett's test with adjustments for multiple comparisons). (f) CRISPRi of the enhancer containing rs72713175 significantly reduced melanin levels in MNT-1 cells (control, n = 18; others, n = 9, Two-sided Dunnett's test with adjustments for multiple comparisons). Data are presented as mean \pm SEM and p values were listed above the bars.



Extended Data Fig. 10. Identification of functional regulatory variants near the *DDB1* locus. (a) Plots showing allelic skewed variants in regulatory elements near the *DDB1* locus. rs7948623 overlaps an open chromatin region in melanocytes and many other cell types. rs2277285 and rs2943806 are located within CTCF binding sites and TAD boundaries. Blue tracks are DNase-Seq, ATAC-Seq, and ChIP-Seq data from melanocytes; orange tracks indicate ChIP-Seq data from melanoma (501-mel) cells; gray tracks indicate CTCF ChIP-Seq data from three cell lines; and green tracks indicate DNase-Seq data from ENCODE⁶⁸. (b-d) Allelic skews at rs7948623, rs2277285 and rs2943806 as estimated by MPRA (n = 3).

P values were estimated with a random effects model for mpralm and paired t-tests without multiple testing adjustments. For boxplots, central lines are median, with boxes extending from the 25th to the 75th percentiles. Whiskers further extend by ± 1.5 times the interquartile range from the limits of each box. (e) rs7948623 disrupts a MITF binding motif and overlaps ChIP-seq peaks from Cistrome database⁷². (f-g) LD pattern between the MFVs near the *DDB1* locus. LD was calculated using the 180G¹⁸ dataset.

Supplementary Material

Refer to Web version on PubMed Central for supplementary material.

Acknowledgements

This research was supported by the following grants: NIH grants 3UM1HG009408–02S1, 1R01GM113657–01 and 5R01AR076241–02. We thank the Skin Biology and Disease Resource-based Center (SBDRC, NIH P30-AR069589) at the University of Pennsylvania for funding and for providing human primary melanocytes. The sequencing of MPRA was carried by the DNA Technologies and Expression Analysis Core at the UC Davis Genome Center, supported by NIH Shared Instrumentation Grant 1S10OD010786–01. We thank Elizabeth Burton for assistance on part of the plasmid cloning. We thank Dr. Zhaolan (Joe) Zhou from the Department of Genetics at UPenn for sharing their tissue culture room. We thank Dr. Jennifer Phillips-Cremens from the Department of Genetics at UPenn for constructive suggestions on Hi-C. We thank Hetty Wong and Hao Wu at the University of Pennsylvania for sharing their experimental equipment. We thank the African participants for their contributions to this study.

Data availability

The epigenomic data, Hi-C and HiChIP data were uploaded to UCSC browser and are available at https://genome.ucsc.edu/s/fengyq/Tishkoff_Lab%2Dhg38%2DMPRA%2DHiC_Pigmentation. All RNA-seq and epigenomic data generated in this study are available at GEO: GSE240717. Genotype data for GWAS was in dbGaP: phs001396.v1.pl.

References including Methods

1. Jablonski NG & Chaplin G Colloquium paper: human skin pigmentation as an adaptation to UV radiation. *Proc. Natl. Acad. Sci. U. S. A.* 107 Suppl 2, 8962–8968 (2010). [PubMed: 20445093]
2. Barsh GS What controls variation in human skin color? *PLoS Biol.* 1, E27 (2003). [PubMed: 14551921]
3. Beleza S et al. Genetic architecture of skin and eye color in an African-European admixed population. *PLoS Genet.* 9, e1003372 (2013). [PubMed: 23555287]
4. Liu F et al. Genetics of skin color variation in Europeans: genome-wide association studies with functional follow-up. *Hum. Genet.* 134, 823–835 (2015). [PubMed: 25963972]
5. Martin AR et al. An Unexpectedly Complex Architecture for Skin Pigmentation in Africans. *Cell* 171, 1340–1353.e14 (2017). [PubMed: 29195075]
6. Galván-Femenía I et al. Multitrait genome association analysis identifies new susceptibility genes for human anthropometric variation in the GCAT cohort. *J. Med. Genet.* 55, 765–778 (2018). [PubMed: 30166351]
7. Nealelab. UK BioBank GWAS. <http://www.nealelab.is/uk-biobank/> <http://www.nealelab.is/uk-biobank/> (2018).
8. Adhikari K et al. A GWAS in Latin Americans highlights the convergent evolution of lighter skin pigmentation in Eurasia. *Nat. Commun.* 10, 358 (2019). [PubMed: 30664655]

9. Lona-Durazo F et al. Meta-analysis of GWA studies provides new insights on the genetic architecture of skin pigmentation in recently admixed populations. *BMC Genet.* 20, 59 (2019). [PubMed: 31315583]
10. Jiang L, Zheng Z, Fang H & Yang J A generalized linear mixed model association tool for biobank-scale data. *Nat. Genet.* 53, 1616–1621 (2021). [PubMed: 34737426]
11. Batai K et al. Genetic loci associated with skin pigmentation in African Americans and their effects on vitamin D deficiency. *PLoS Genet.* 17, e1009319 (2021). [PubMed: 33600456]
12. Pairo-Castineira E et al. Expanded analysis of pigmentation genetics in UK Biobank. *bioRxiv* (2022) doi:10.1101/2022.01.30.478418.
13. Crawford NG et al. Loci associated with skin pigmentation identified in African populations. *Science* 358, (2017).
14. Miller CT et al. cis-Regulatory changes in Kit ligand expression and parallel evolution of pigmentation in sticklebacks and humans. *Cell* 131, 1179–1189 (2007). [PubMed: 18083106]
15. Tsetsckhladze ZR et al. Functional assessment of human coding mutations affecting skin pigmentation using zebrafish. *PLoS One* 7, e47398 (2012). [PubMed: 23071798]
16. Visser M, Kayser M & Palstra R-J HERC2 rs12913832 modulates human pigmentation by attenuating chromatin-loop formation between a long-range enhancer and the OCA2 promoter. *Genome Res.* 22, 446–455 (2012). [PubMed: 22234890]
17. Praetorius C et al. A polymorphism in IRF4 affects human pigmentation through a tyrosinase-dependent MITF/TFAP2A pathway. *Cell* 155, 1022–1033 (2013). [PubMed: 24267888]
18. Fan S et al. Whole-genome sequencing reveals a complex African population demographic history and signatures of local adaptation. *Cell* 186, 923–939.e14 (2023). [PubMed: 36868214]
19. Gordon MG et al. lentiMPRA and MPRAflow for high-throughput functional characterization of gene regulatory elements. *Nat. Protoc.* 15, 2387–2412 (2020). [PubMed: 32641802]
20. Akey JM et al. Tracking footprints of artificial selection in the dog genome. *Proc. Natl. Acad. Sci. U. S. A.* 107, 1160–1165 (2010). [PubMed: 20080661]
21. Myint L, Avramopoulos DG, Goff LA & Hansen KD Linear models enable powerful differential activity analysis in massively parallel reporter assays. *BMC Genomics* 20, 209 (2019). [PubMed: 30866806]
22. Adelman CH et al. MFSD12 mediates the import of cysteine into melanosomes and lysosomes. *Nature* 588, 699–704 (2020). [PubMed: 33208952]
23. Luecke S et al. The aryl hydrocarbon receptor (AHR), a novel regulator of human melanogenesis. *Pigment Cell Melanoma Res.* 23, 828–833 (2010). [PubMed: 20973933]
24. Kayser M et al. Three genome-wide association studies and a linkage analysis identify HERC2 as a human iris color gene. *Am. J. Hum. Genet.* 82, 411–423 (2008). [PubMed: 18252221]
25. Lona-Durazo F et al. A large Canadian cohort provides insights into the genetic architecture of human hair colour. *Commun. Biol.* 4, 1253 (2021). [PubMed: 34737440]
26. Simcoe M et al. Genome-wide association study in almost 195,000 individuals identifies 50 previously unidentified genetic loci for eye color. *Sci. Adv.* 7, eabd1239 (2021). [PubMed: 33692100]
27. Liang Z et al. BL-Hi-C is an efficient and sensitive approach for capturing structural and regulatory chromatin interactions. *Nat. Commun.* 8, 1622 (2017). [PubMed: 29158486]
28. Mumbach MR et al. HiChIP: efficient and sensitive analysis of protein-directed genome architecture. *Nat. Methods* 13, 919–922 (2016). [PubMed: 27643841]
29. Bhattacharyya S, Chandra V, Vijayanand P & Ay F Identification of significant chromatin contacts from HiChIP data by FitHiChIP. *Nat. Commun.* 10, 4221 (2019). [PubMed: 31530818]
30. Ochoa D et al. Open Targets Platform: supporting systematic drug-target identification and prioritisation. *Nucleic Acids Res.* 49, D1302–D1310 (2021). [PubMed: 33196847]
31. 1000 Genomes Project Consortium et al. A global reference for human genetic variation. *Nature* 526, 68–74 (2015). [PubMed: 26432245]
32. Albers PK & McVean G Dating genomic variants and shared ancestry in population-scale sequencing data. *PLoS Biol.* 18, e3000586 (2020). [PubMed: 31951611]

33. Levy C, Khaled M & Fisher DE MITF: master regulator of melanocyte development and melanoma oncogene. *Trends Mol. Med.* 12, 406–414 (2006). [PubMed: 16899407]
34. Klein JC et al. A systematic evaluation of the design and context dependencies of massively parallel reporter assays. *Nat. Methods* 17, 1083–1091 (2020). [PubMed: 33046894]
35. Tan B et al. FOXP3 over-expression inhibits melanoma tumorigenesis via effects on proliferation and apoptosis. *Oncotarget* 5, 264–276 (2014). [PubMed: 24406338]
36. Cao Y et al. Accurate loop calling for 3D genomic data with cLoops. *Bioinformatics* 36, 666–675 (2020). [PubMed: 31504161]
37. Takeda K et al. Induction of melanocyte-specific microphthalmia-associated transcription factor by Wnt-3a. *J. Biol. Chem.* 275, 14013–14016 (2000). [PubMed: 10747853]
38. Bondurand N et al. Interaction among SOX10, PAX3 and MITF, three genes altered in Waardenburg syndrome. *Hum. Mol. Genet.* 9, 1907–1917 (2000). [PubMed: 10942418]
39. Kichaev G et al. Leveraging Polygenic Functional Enrichment to Improve GWAS Power. *Am. J. Hum. Genet.* 104, 65–75 (2019). [PubMed: 30595370]
40. Morgan MD et al. Genome-wide study of hair colour in UK Biobank explains most of the SNP heritability. *Nat. Commun.* 9, 5271 (2018). [PubMed: 30531825]
41. Visconti A et al. Genome-wide association study in 176,678 Europeans reveals genetic loci for tanning response to sun exposure. *Nat. Commun.* 9, 1684 (2018). [PubMed: 29739929]
42. Larimore J et al. Mutations in the BLOC-1 subunits dysbindin and muted generate divergent and dosage-dependent phenotypes. *J. Biol. Chem.* 289, 14291–14300 (2014). [PubMed: 24713699]
43. Saito H et al. Melanocyte-specific microphthalmia-associated transcription factor isoform activates its own gene promoter through physical interaction with lymphoid-enhancing factor 1. *J. Biol. Chem.* 277, 28787–28794 (2002). [PubMed: 12048204]
44. Wang X et al. LEF-1 Regulates Tyrosinase Gene Transcription In Vitro. *PLoS One* 10, e0143142 (2015). [PubMed: 26580798]
45. Ishitani T et al. The TAK1-NLK-MAPK-related pathway antagonizes signalling between beta-catenin and transcription factor TCF. *Nature* 399, 798–802 (1999). [PubMed: 10391247]
46. Ishitani T, Ninomiya-Tsuji J & Matsumoto K Regulation of lymphoid enhancer factor 1/T-cell factor by mitogen-activated protein kinase-related Nemo-like kinase-dependent phosphorylation in Wnt/beta-catenin signaling. *Mol. Cell. Biol.* 23, 1379–1389 (2003). [PubMed: 12556497]
47. Gai Z, Gui T & Muragaki Y The function of TRPS1 in the development and differentiation of bone, kidney, and hair follicles. *Histol. Histopathol.* 26, 915–921 (2011). [PubMed: 21630221]
48. Swoboda A et al. STAT3 promotes melanoma metastasis by CEBP-induced repression of the MITF pathway. *Oncogene* 40, 1091–1105 (2021). [PubMed: 33323974]
49. Mallick S et al. The Simons Genome Diversity Project: 300 genomes from 142 diverse populations. *Nature* 538, 201–206 (2016). [PubMed: 27654912]
50. Sitaram A & Marks MS Mechanisms of protein delivery to melanosomes in pigment cells. *Physiology (Bethesda)* 27, 85–99 (2012). [PubMed: 22505665]
51. Wang Z et al. CYB561A3 is the key lysosomal iron reductase required for Burkitt B-cell growth and survival. *Blood* 138, 2216–2230 (2021). [PubMed: 34232987]
52. Karlsson M et al. A single-cell type transcriptomics map of human tissues. *Sci. Adv.* 7, eabh2169 (2021). [PubMed: 34321199]
53. Lee JH et al. Evolutionarily assembled cis-regulatory module at a human ciliopathy locus. *Science* 335, 966–969 (2012). [PubMed: 22282472]
54. Lamason RL et al. SLC24A5, a putative cation exchanger, affects pigmentation in zebrafish and humans. *Science* 310, 1782–1786 (2005). [PubMed: 16357253]
55. Lavado A, Olivares C, García-Borrón JC & Montoliu L Molecular basis of the extreme dilution mottled mouse mutation: a combination of coding and noncoding genomic alterations. *J. Biol. Chem.* 280, 4817–4824 (2005). [PubMed: 15572362]
56. Seruggia D, Fernández A, Cantero M, Pelczar P & Montoliu L Functional validation of mouse tyrosinase non-coding regulatory DNA elements by CRISPR-Cas9-mediated mutagenesis. *Nucleic Acids Res.* 43, 4855–4867 (2015). [PubMed: 25897126]

57. Ambrosio AL, Boyle JA, Aradi AE, Christian KA & Di Pietro SM TPC2 controls pigmentation by regulating melanosome pH and size. *Proc. Natl. Acad. Sci. U. S. A.* 113, 5622–5627 (2016). [PubMed: 27140606]
58. Ploper D et al. MITF drives endolysosomal biogenesis and potentiates Wnt signaling in melanoma cells. *Proc. Natl. Acad. Sci. U. S. A.* 112, E420–9 (2015). [PubMed: 25605940]
59. Zhang Y et al. Lef1 contributes to the differentiation of bulge stem cells by nuclear translocation and cross-talk with the Notch signaling pathway. *Int. J. Med. Sci.* 10, 738–746 (2013). [PubMed: 23630438]
60. Fantauzzo KA, Kurban M, Levy B & Christiano AM Trps1 and its target gene Sox9 regulate epithelial proliferation in the developing hair follicle and are associated with hypertrichosis. *PLoS Genet.* 8, e1003002 (2012). [PubMed: 23133399]
61. Fantauzzo KA & Christiano AM Trps1 activates a network of secreted Wnt inhibitors and transcription factors crucial to vibrissa follicle morphogenesis. *Development* 139, 203–214 (2012). [PubMed: 22115758]
62. Yamada T et al. Wnt/ β -catenin and kit signaling sequentially regulate melanocyte stem cell differentiation in UVB-induced epidermal pigmentation. *J. Invest. Dermatol.* 133, 2753–2762 (2013). [PubMed: 23702581]
63. Andl T, Reddy ST, Gaddapara T & Millar SE WNT signals are required for the initiation of hair follicle development. *Dev. Cell* 2, 643–653 (2002). [PubMed: 12015971]
64. Tobias PV & Biesele M The Bushmen: San Hunters and Herders of Southern Africa. (Human & Rousseau, 1978).
65. Feng Y, McQuillan MA & Tishkoff SA Evolutionary genetics of skin pigmentation in African populations. *Hum. Mol. Genet.* 30, R88–R97 (2021). [PubMed: 33438000]
66. Rawofi L et al. Genome-wide association study of pigmentary traits (skin and iris color) in individuals of East Asian ancestry. *PeerJ* 5, e3951 (2017). [PubMed: 29109912]
67. Stokowski RP et al. A genomewide association study of skin pigmentation in a South Asian population. *Am. J. Hum. Genet.* 81, 1119–1132 (2007). [PubMed: 17999355]
68. ENCODE Project Consortium. An integrated encyclopedia of DNA elements in the human genome. *Nature* 489, 57–74 (2012). [PubMed: 22955616]
69. Coetsee SG, Coetsee GA & Hazelett DJ motifbreakR: an R/Bioconductor package for predicting variant effects at transcription factor binding sites. *Bioinformatics* 31, 3847–3849 (2015). [PubMed: 26272984]
70. Shin J-H, Blay S, Graham J & McNeney B LDheatmap: AnRFunction for Graphical Display of Pairwise Linkage Disequilibria Between Single Nucleotide Polymorphisms. *J. Stat. Softw.* 16, (2006).
71. An L et al. OnTAD: hierarchical domain structure reveals the divergence of activity among TADs and boundaries. *Genome Biol.* 20, 282 (2019). [PubMed: 31847870]
72. Liu T et al. Cistrome: an integrative platform for transcriptional regulation studies. *Genome Biol.* 12, R83 (2011). [PubMed: 21859476]
73. Kang HM et al. Variance component model to account for sample structure in genome-wide association studies. *Nat. Genet.* 42, 348–354 (2010). [PubMed: 20208533]
74. Hyun Min Kang E et al. Efficient and Parallelizable Association Container Toolbox, EPACTS v3.3.0. EPACTS <http://genome.sph.umich.edu/wiki/EPACTS>.
75. Bhatia G, Patterson N, Sankararaman S & Price AL Estimating and interpreting FST: the impact of rare variants. *Genome Res.* 23, 1514–1521 (2013). [PubMed: 23861382]
76. McLean CY et al. GREAT improves functional interpretation of cis-regulatory regions. *Nat. Biotechnol.* 28, 495–501 (2010). [PubMed: 20436461]
77. Watanabe K, Taskesen E, van Bochoven A & Posthuma D Functional mapping and annotation of genetic associations with FUMA. *Nat. Commun.* 8, 1826 (2017). [PubMed: 29184056]
78. Barrett T et al. NCBI GEO: mining millions of expression profiles--database and tools. *Nucleic Acids Res.* 33, D562–6 (2005). [PubMed: 15608262]
79. Dickinson ME et al. High-throughput discovery of novel developmental phenotypes. *Nature* 537, 508–514 (2016). [PubMed: 27626380]

80. Baxter LL, Watkins-Chow DE, Pavan WJ & Loftus SK A curated gene list for expanding the horizons of pigmentation biology. *Pigment Cell Melanoma Res.* 32, 348–358 (2019). [PubMed: 30339321]
81. Uhlen M et al. A pathology atlas of the human cancer transcriptome. *Science* 357, (2017).
82. Mago T & Salzberg SL FLASH: fast length adjustment of short reads to improve genome assemblies. *Bioinformatics* 27, 2957–2963 (2011). [PubMed: 21903629]
83. Chen S, Zhou Y, Chen Y & Gu J fastp: an ultra-fast all-in-one FASTQ preprocessor. *Bioinformatics* 34, i884–i890 (2018). [PubMed: 30423086]
84. Bray NL, Pimentel H, Melsted P & Pachter L Near-optimal probabilistic RNA-seq quantification. *Nat. Biotechnol.* 34, 525–527 (2016). [PubMed: 27043002]
85. Sonesson C, Love MI & Robinson MD Differential analyses for RNA-seq: transcript-level estimates improve gene-level inferences. *F1000Res.* 4, 1521 (2015). [PubMed: 26925227]
86. Love MI, Huber W & Anders S Moderated estimation of fold change and dispersion for RNA-seq data with DESeq2. *Genome Biol.* 15, 550 (2014). [PubMed: 25516281]
87. Kucukural A, Yukselen O, Ozata DM, Moore MJ & Garber M DEBrowser: interactive differential expression analysis and visualization tool for count data. *BMC Genomics* 20, 6 (2019). [PubMed: 30611200]
88. Blighe K Lewis Rana S. EnhancedVolcano: Publication-ready volcano plots with enhanced colouring and labeling. R package version 1.14.0. EnhancedVolcano <https://github.com/kevinblighe/EnhancedVolcano>.
89. Luo W & Brouwer C Pathview: an R/Bioconductor package for pathway-based data integration and visualization. *Bioinformatics* 29, 1830–1831 (2013). [PubMed: 23740750]
90. Corces MR et al. An improved ATAC-seq protocol reduces background and enables interrogation of frozen tissues. *Nat. Methods* 14, 959–962 (2017). [PubMed: 28846090]
91. Langmead B & Salzberg SL Fast gapped-read alignment with Bowtie 2. *Nat. Methods* 9, 357–359 (2012). [PubMed: 22388286]
92. McKenna A et al. The Genome Analysis Toolkit: a MapReduce framework for analyzing next-generation DNA sequencing data. *Genome Res.* 20, 1297–1303 (2010). [PubMed: 20644199]
93. Li H et al. The Sequence Alignment/Map format and SAMtools. *Bioinformatics* 25, 2078–2079 (2009). [PubMed: 19505943]
94. Ramírez F et al. deepTools2: a next generation web server for deep-sequencing data analysis. *Nucleic Acids Res.* 44, W160–5 (2016). [PubMed: 27079975]
95. Zhang Y et al. Model-based analysis of ChIP-Seq (MACS). *Genome Biol.* 9, R137 (2008). [PubMed: 18798982]
96. Liao Y, Smyth GK & Shi W featureCounts: an efficient general purpose program for assigning sequence reads to genomic features. *Bioinformatics* 30, 923–930 (2014). [PubMed: 24227677]
97. Meers MP, Tenenbaum D & Henikoff S Peak calling by Sparse Enrichment Analysis for CUT&RUN chromatin profiling. *Epigenetics Chromatin* 12, 42 (2019). [PubMed: 31300027]
98. Kulakovskiy IV et al. HOCOMOCO: towards a complete collection of transcription factor binding models for human and mouse via large-scale ChIP-Seq analysis. *Nucleic Acids Res.* 46, D252–D259 (2018). [PubMed: 29140464]

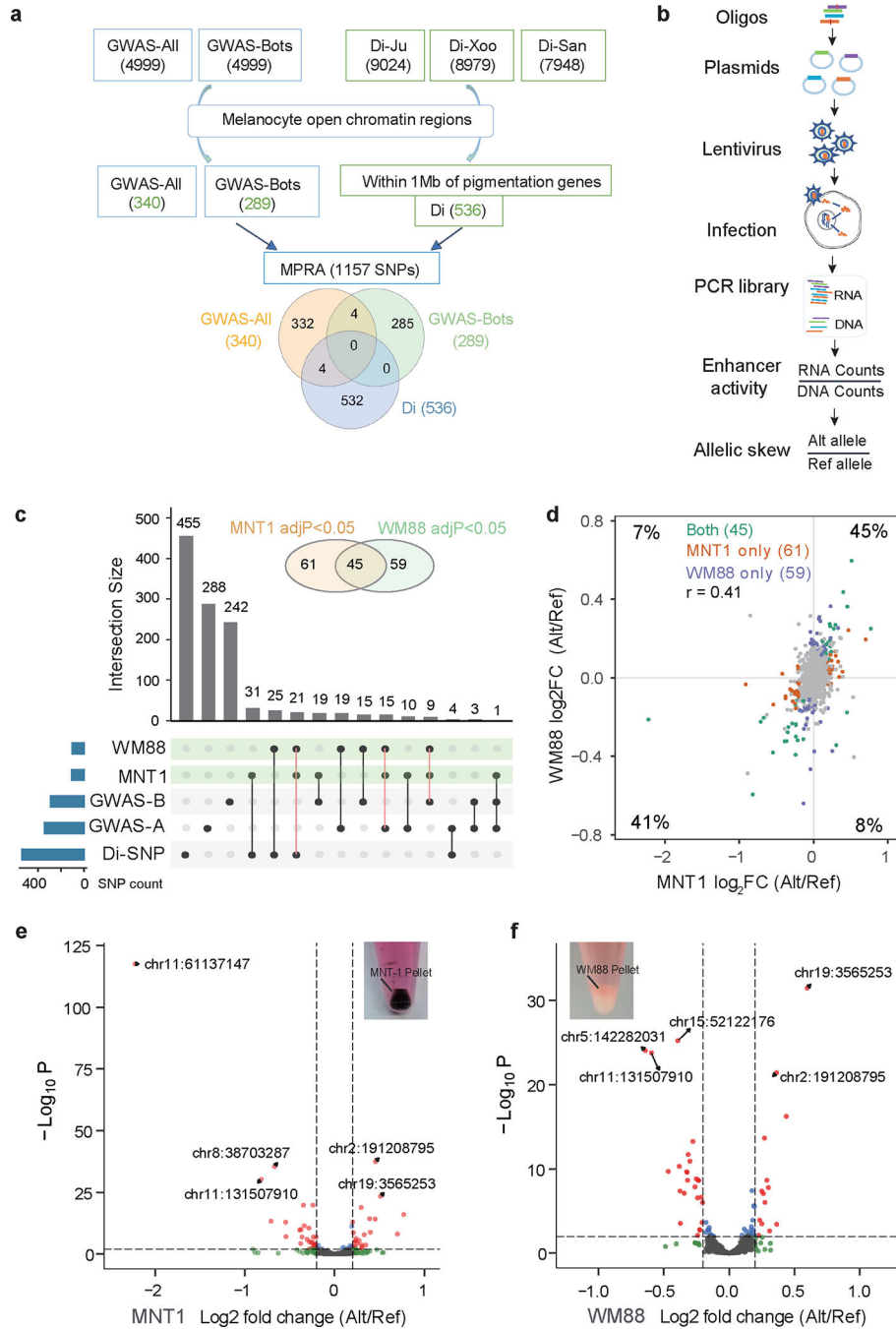


Fig. 1: Massively parallel screening of genetic variants associated with African skin pigmentation.

(a) Selection of candidate regulatory variants. GWAS-All, top 4999 SNPs from GWAS of skin pigmentation in Africans ($p < 2.3 \times 10^{-4}$); GWAS-Bots, top 4999 SNPs from GWAS of skin pigmentation in Botswana ($p < 1.7 \times 10^{-4}$); Di-Ju are top 0.1% Di-SNPs from the Ju|hoansi versus other populations without inclusion of the !Xoo; Di-Xoo are top 0.1% Di-SNPs from the !Xoo versus other populations without inclusion of the Ju|hoansi; Di-San are top 0.1% Di-SNPs from the Ju|hoansi and the !Xoo versus other populations. (b)

Schematic of lentiMPRA workflow. **(c)** Upset plot showing the intersections of significant allelic skewed variants from GWAS and Di analysis in MNT-1 and WM88. Alleles with significant differential regulatory activities (adjusted p-value < 0.05) in both MNT-1 and WM88 are highlighted with orange solid lines. GWAS_A represents GWAS-All; GWAS_B represents GWAS-Bots. **(d)** Comparison of allelic skews in two melanoma cell lines (MNT-1 and WM88). The percentages are defined by the number of SNPs in each quadrant / total number of SNPs. Alleles with significant differential regulatory activities (adjusted p-value < 0.05) in both cell lines (green), MNT-1 (orange), and WM88 (blue) are highlighted. Nonsignificant alleles are colored in gray. The correlation of allelic skews in MNT-1 and WM88 is estimated by Pearson's $r = 0.41$, $p = 2.6 \times 10^{-46}$. **(e-f)** Volcano plots showing allelic skewed variants in MNT-1 and WM88. Allelic skew is defined as the log₂ fold change of the enhancer activity between the alternative and reference alleles (reference alleles match the genome hg19). The location of the top 5 SNPs based on the hg19 reference genome are highlighted. Pictures of the cell pellets of MNT-1 and WM88 showing that MNT-1 are darkly pigmented and WM88 are near non-pigmented.

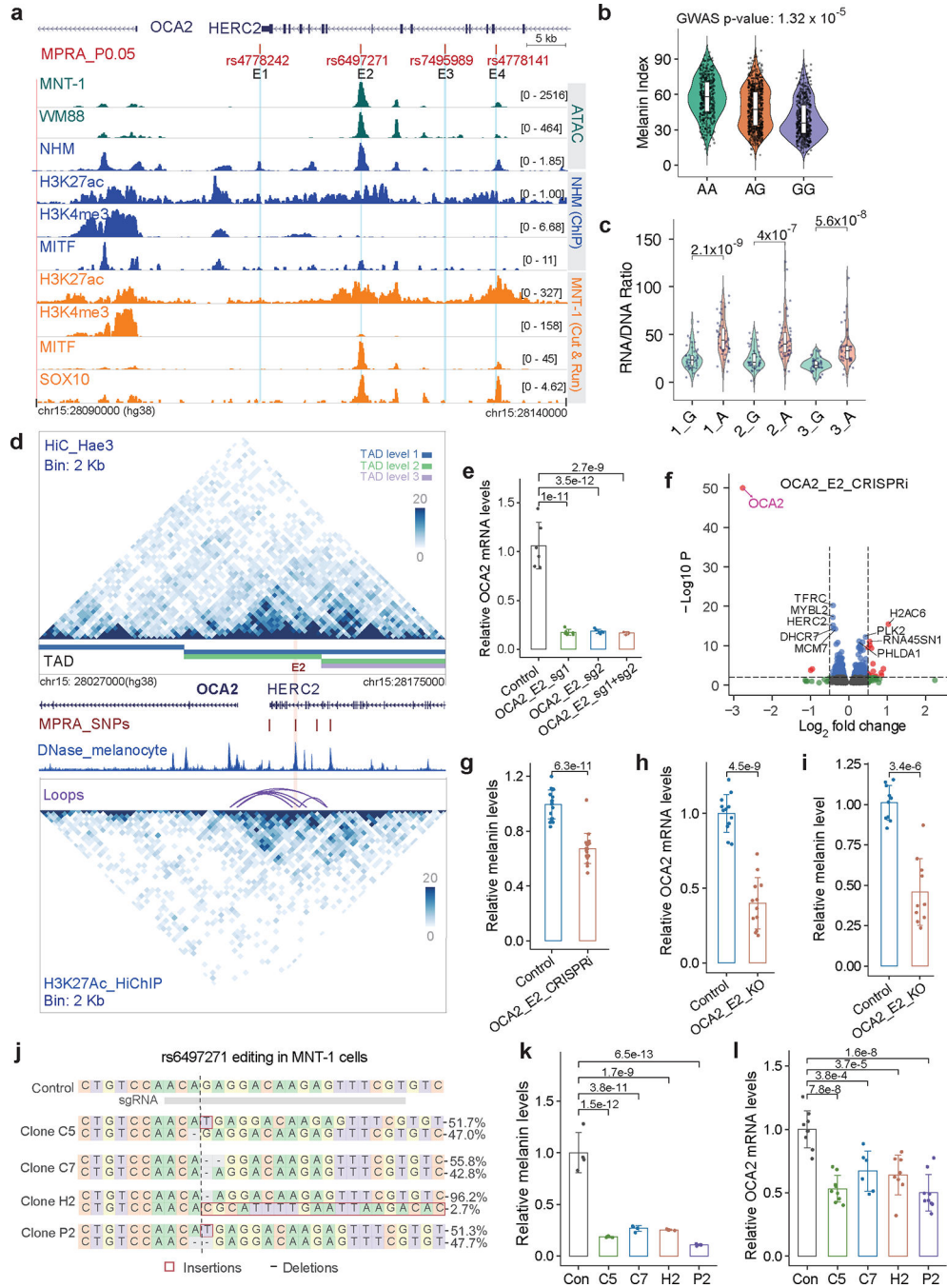


Fig. 2: rs6497271 impacts *OCA2* expression and contributes to human skin color variations. (a) MPRA identified four regulatory variants near *OCA2*. (b) rs6497271 is associated with African skin pigmentation (n = 1544), p-value was calculated using EPACTS “q. emmax” method. (c) MPRA showed that rs6497271 significantly changed the enhancer activities in MNT-1. Two-tailed unpaired t-tests (three biological replicates). (d) Chromatin interactions near *OCA2* identified by Hi-C and H3K27ac HiChIP using Hae3 digestion. The purple arches are chromatin loops, the four vertical red lines are MFVs, the pink shadowed line represents enhancer E2. (e) qPCR showed that CRISPRi of E2 significantly reduces the

expression of *OCA2*. CRISPRi was performed in MNT-1. Two-sided Dunnett's test with adjustments for multiple comparisons (group OCA2_E2_sg1+sg2, n = 3; other groups, n = 6). **(f)** RNA-Seq data showing CRISPRi of E2 inhibits *OCA2* gene expression. The p-value of *OCA2* ($p = 0$) was set to 1×10^{-50} to be shown in the plot. p-values were calculated using DESeq2. **(g)** CRISPRi of E2 significantly reduced melanin levels. The CRISPRi was performed in MNT-1 using two sgRNAs. Two-tailed unpaired t-tests (n = 19). **(h)** qPCR showed that CRISPR-KO of E2 significantly decreases the expression level of *OCA2*. The CRISPR-KO was performed in MNT-1 using two sgRNAs. Two-tailed unpaired t-tests (n = 12). **(i)** CRISPR-KO of E2 significantly reduced melanin levels. Two-tailed unpaired t-tests (n = 10). **(j)** Genotyping of four CRISPR-edited MNT-1 clones at rs6497271. The 395bp amplicons flanking rs6497271 were amplified and sequenced using MiSeq. Top 2 genotypes in each clone are shown. **(k)** Mutations near rs6497271 significantly decreased melanin levels in MNT-1. Four clones were selected and compared with non-edited control cells. Two-sided Dunnett's test with adjustments for multiple comparisons (n = 4). **(l)** Mutations near rs6497271 significantly reduced the expression of *OCA2* in MNT-1. Two-sided Dunnett's test with adjustments for multiple comparisons (OCA2-E2_C7, n = 6; OCA2-E2_H2, n = 8; others, n = 9). Data were presented as mean \pm SEM. P values were listed above the bars. For boxplots, central lines are median, with boxes extending from the 25th to the 75th percentiles. Whiskers further extend by ± 1.5 times the interquartile range from the limits of each box.

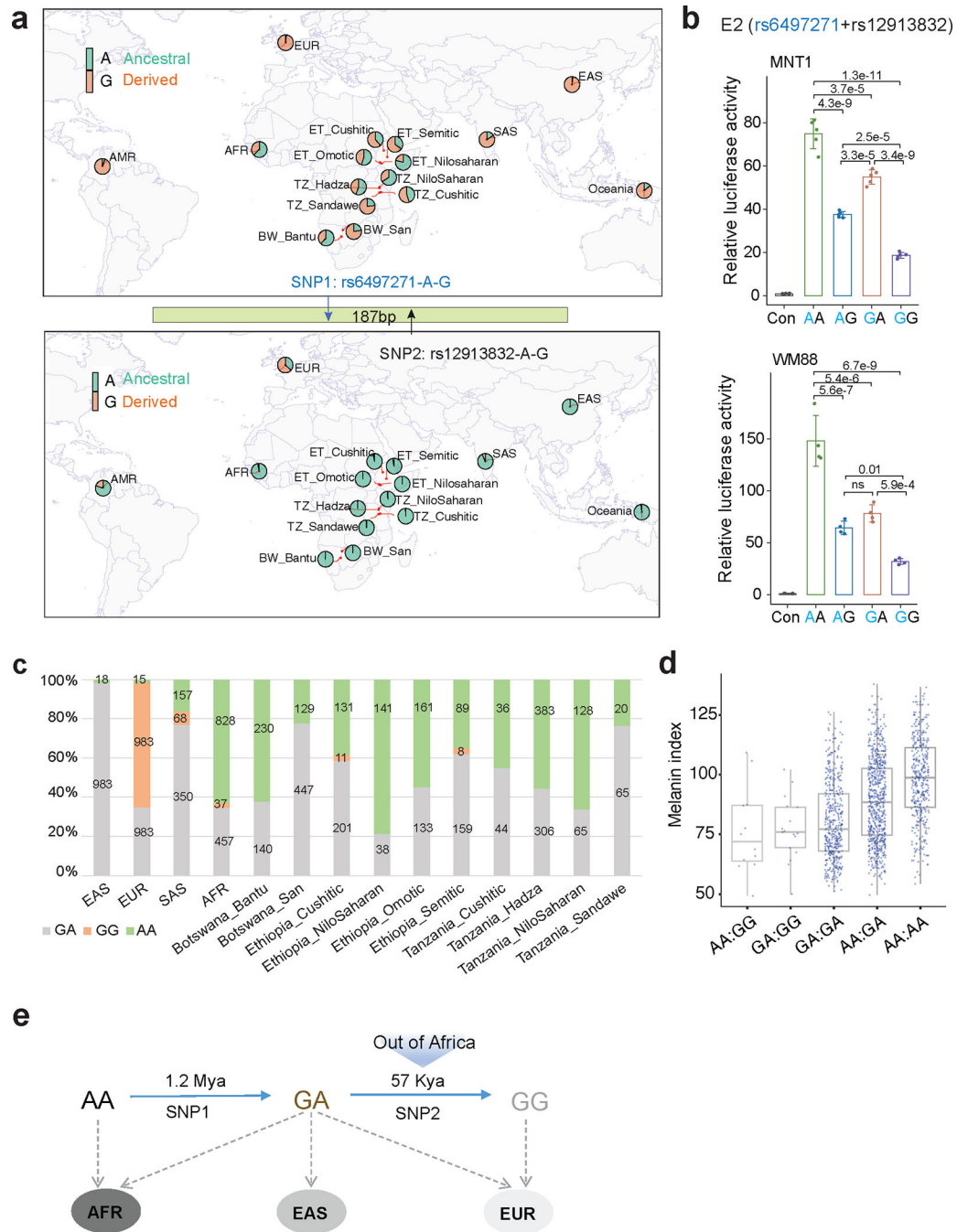


Fig. 3: Continuing evolution of *OCA2* enhancer E2 contributes to African skin pigmentation diversity.

(a) Allele frequencies at rs6497271 and rs12913832 in global populations. Derived alleles are colored in orange. Data was merged from 1000G³¹, African 5M¹³ and SGDP⁴⁹ datasets. (b) The enhancer activities of 4 haplotypes containing rs6497271 and rs12913832 in MNT-1 and WM88 estimated by LRA. Two-sided Tukey's test with adjustments for multiple comparisons ($n = 4$). Data were presented as mean \pm SEM. ns $p > 0.05$. (c) The frequencies of haplotypes containing rs6497271 and rs12913832 in global populations. Data

was merged from 1000G, African 5M array and SGDP datasets. **(d)** Melanin indexes of individuals with different haplotype combinations at rs6497271 and rs12913832. Data was from GWAS-All (n = 1544). **(e)** Estimated ages of SNP rs6497271 and rs12913832. Data was from <https://human.genome.dating/>. For boxplots, central lines are median, with boxes extending from the 25th to the 75th percentiles. Whiskers further extend by ± 1.5 times the interquartile range from the limits of each box.

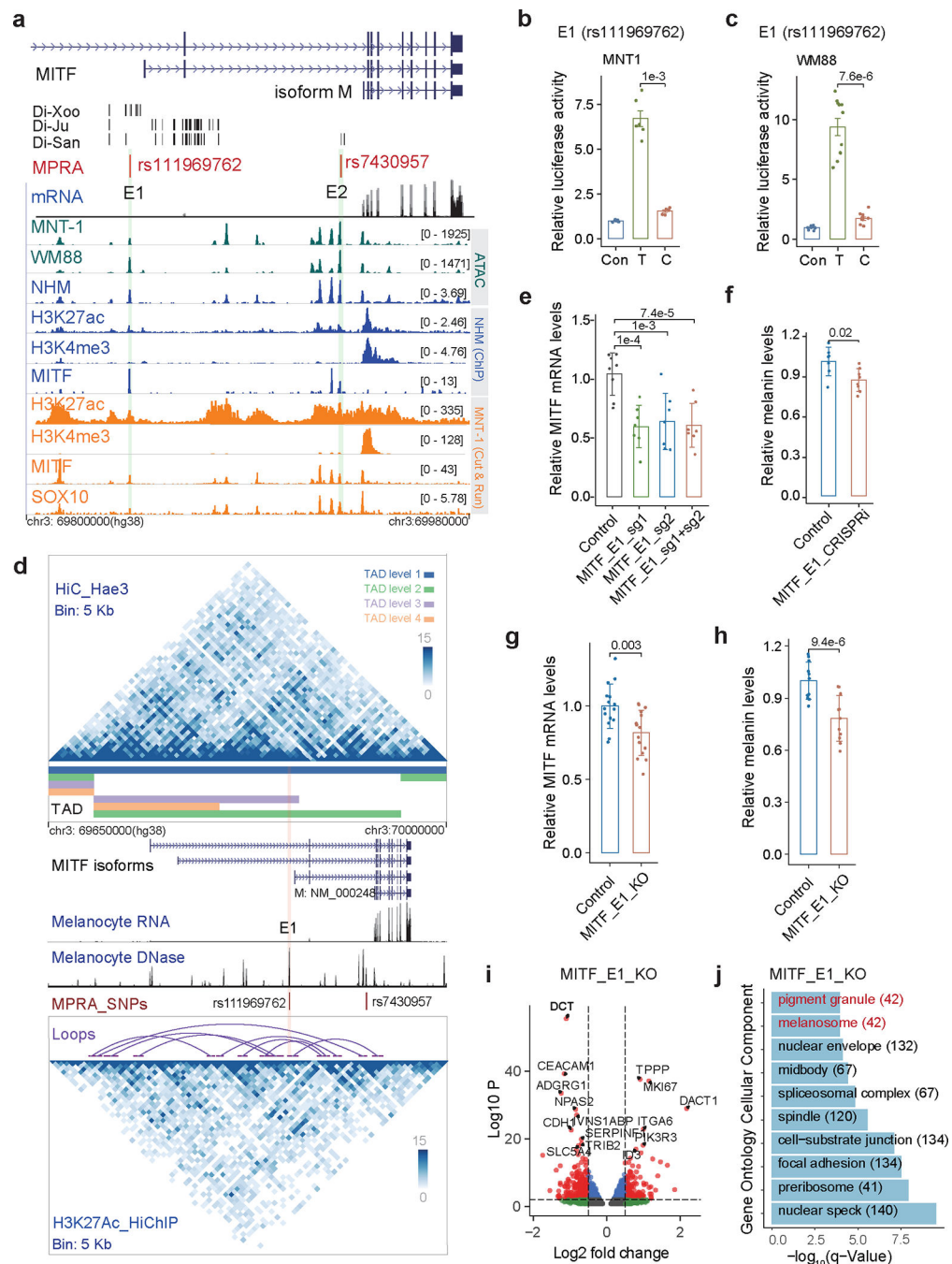


Fig. 4: Regulatory variant rs111969762 near *MITF* contributes to the light skin color of the San. (a) MPRA identified two MFVs in regulatory elements near *MITF*. Di-Ju, Di-Xoo and Di-San are Di-SNPs. Green tracks represent ATAC-seq for MNT-1 and WM88; blue tracks show ATAC-Seq and ChIP-Seq data from normal human melanocytes (NHM); orange tracks indicate CUT&RUN data from MNT-1. The black dashes are Di-SNPs, the light green shadowed regions represent enhancers E1 and E2. (b-c) LRAs showed that rs111969762 located in E1 affects enhancer activity in both MNT-1 and WM88. Two-tailed paired t-tests (MNT-1, n = 6; WM88, n = 11). (d) Chromatin interactions at the *MITF* locus

identified by Hi-C and H3K27ac HiChIP using Hae3 digestion. The upper matrix is from MNT-1 Hi-C data, and the lower matrix is from MNT-1 H3K27ac HiChIP data. TADs were called by onTAD and colored by nested TAD levels. The purple arches were loops called by cLoops. Melanocyte RNA-Seq and DNase-Seq tracks were downloaded from ENCODE⁶⁸. The pink shadowed region represents enhancers E1. **(e)** qPCR showed that CRISPRi of E1 significantly reduces the gene expression of *MITF*. Two-sided Dunnett's test with adjustments for multiple comparisons (control, n = 8; others, n = 7). **(f)** CRISPRi of E1 significantly reduces melanin levels. Two-tailed unpaired t-tests (control, n = 7; MITF_E1_CRISPRi, n = 8). **(g)** qPCR showed that CRISPR-mediated deletion of E1 significantly decreased the gene expression of *MITF*. Two-tailed unpaired t-tests (n = 15). **(h)** CRISPR-mediated deletion of E1 significantly reduced melanin levels (two-tailed unpaired t-tests (n = 8)). CRISPR was performed in MNT-1 using two sgRNAs. **(i)** RNA-Seq data showing differentially expressed genes in E1-deleted MNT-1. Genes plotted in this figure were selected using DESeq2 (p<0.05, three biological replicates). **(j)** Gene ontology analysis of differentially expressed genes in E1-deleted MNT-1. Data were presented as mean \pm SEM. P values were listed above the bars.

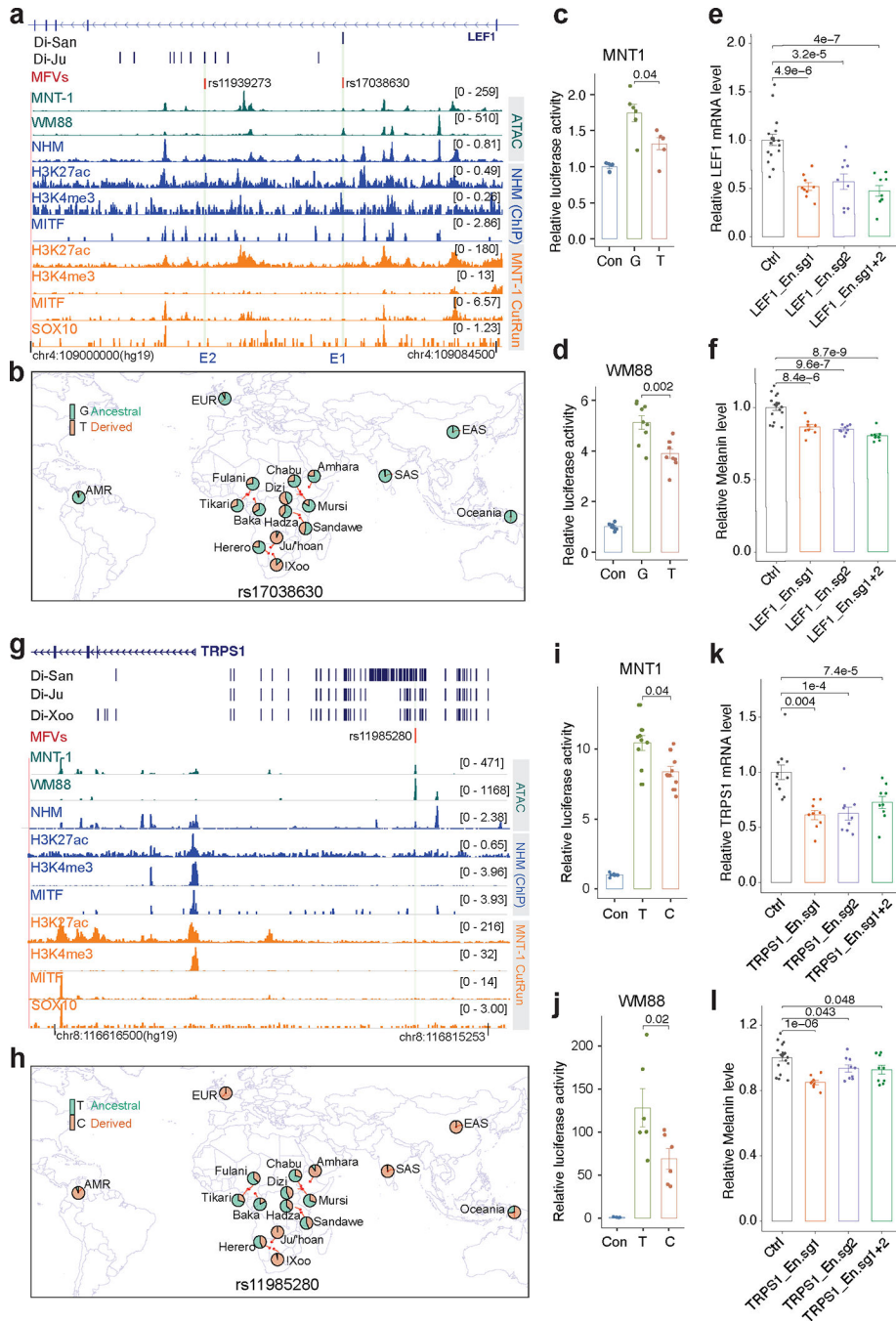


Fig. 5: Regulatory SNPs of *LEF1* and *TRPS1* contribute to the light skin color of the San. (a) MPRA identified two MFVs near the *LEF1* locus. Green tracks represent ATAC-seq for MNT-1 and WM88; blue tracks show ATAC-Seq and ChIP-Seq data from normal human melanocytes (NHM); orange tracks indicate CUT&RUN data from MNT-1. The black dashes are Di-SNPs, the light green shadowed regions represent the locations of enhancers E1 and E2. (b) The allele frequency at rs17038630 in global populations using data from the 1000G³¹, African 5M¹³ and SGDP⁴⁹ datasets. (c-d) LRAs showed that rs17038630 located in E1 affects enhancer activity in both MNT-1 and WM88 (two-tailed paired t-tests

(MNT-1, n = 6; WM88, n = 9)). (e) qPCR showed that CRISPRi of E1 significantly reduces the gene expression of *LEFI*. Two-sided Dunnett's test with adjustments for multiple comparisons (control, n=17; others, n = 9). (f) CRISPRi of E1 significantly reduces melanin levels. Two-sided Dunnett's test with adjustments for multiple comparisons (control, n=18; others, n = 9). (g) MPRA identified one MFV near the *TRPS1* locus. (h) The allele frequency at rs11985280 in global populations, data were from the 180G¹⁸, SGDP⁴⁹ and 1000G³¹ datasets. (i-j) LRAs showed that rs11985280 located in E1 affects enhancer activity in both MNT-1 and WM88 (Two-tailed paired t-tests (MNT-1, n = 9; WM88, n = 6)). (k) qPCR showed that CRISPRi of the enhancer harboring rs11985280 significantly reduces the gene expression of *TRPS1*. Two-sided Dunnett's test with adjustments for multiple comparisons (control, n=11; others, n = 9). (l) CRISPRi of the enhancer harboring rs11985280 significantly reduces melanin levels. Two-tailed unpaired t-tests (control, n=18; others, n = 9). Data were presented as mean \pm SEM, P values were listed above the bars.

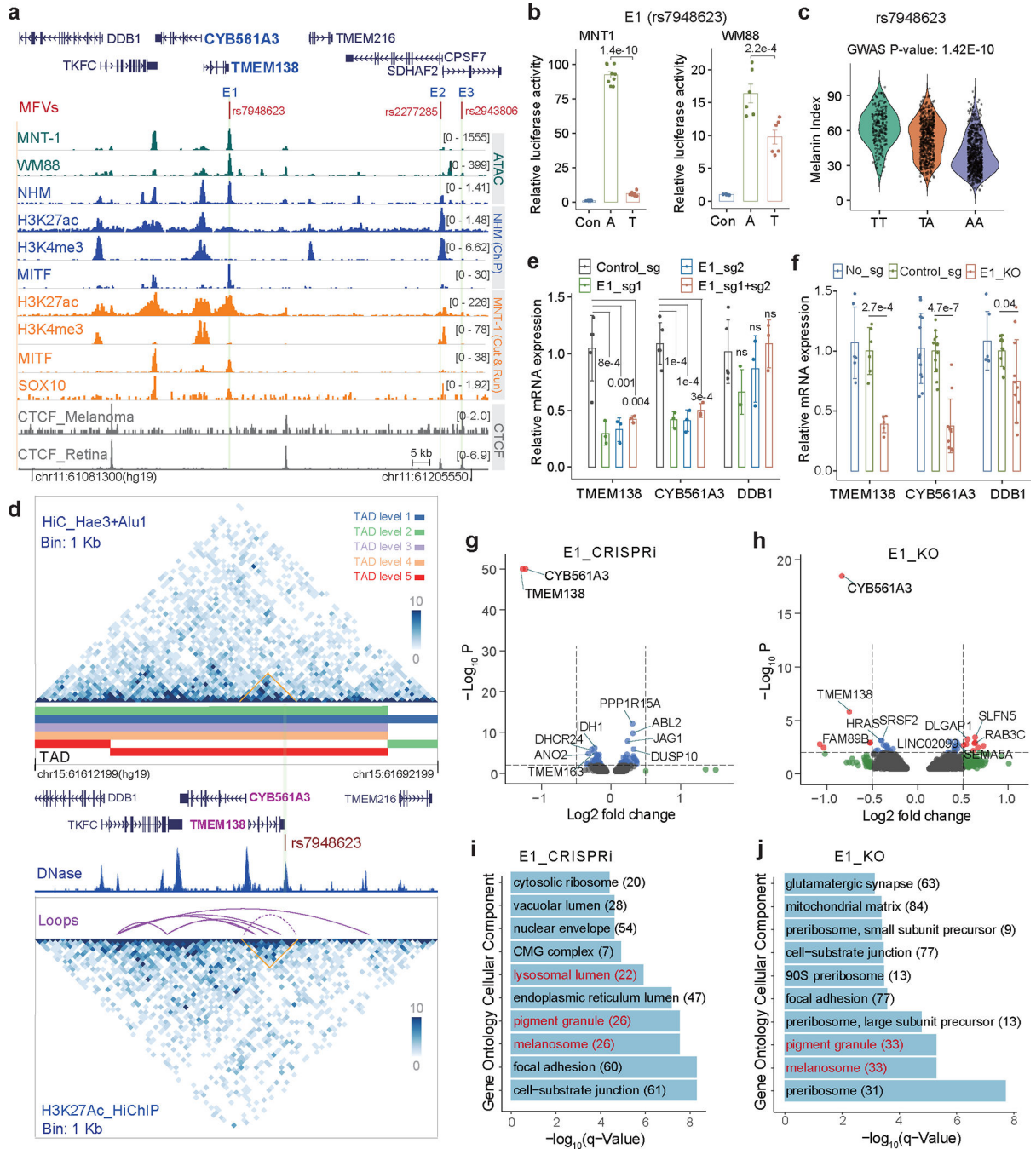


Fig. 6: *CYB561A3* and *TMEM138* are the primary target genes of GWAS-SNP rs7948623. (a) Three regulatory variants identified by MPRA near the *DDB1* locus. The red dashes are MFVs, and the light green shadowed regions represent enhancers E1, E2 and E3. (b) LRA showed that rs7948623 affects enhancer activity. Two-tailed paired t-tests, MNT-1 (n = 9), WM88 (n = 6). (c) The allele A at rs7948623 is associated with light skin color in Africans (n = 1544), p-value was calculated using EPACTS “q. emmax” method. (d) Chromatin interactions near *DDB1* identified by Hi-C and H3K27ac HiChIP. The light green shadowed regions represent enhancers E1 and the interaction matrix between E1 and

its targets were highlighted by orange triangles. (e) qPCR showed that CRISPRi of E1 in MNT-1 significantly decreases the expression of *CYB561A3* and *TMEM138* (Two-sided Dunnett's test with adjustments for multiple comparisons (control sgRNA n = 5; others n = 3)). (f) qPCR showed that CRISPR-mediated deletion of E1 significantly decreases the gene expression of *CYB561A3*, *TMEM138* and *DDB1*. Two-tailed unpaired t-tests without adjustments for multiple comparisons (in group No_sg, *TMEM138* (n = 6), *CYB561A3* (n = 12), *DDB1* (n = 6); in group Control_sg, *TMEM138* (n = 6), *CYB561A3* (n = 12), *DDB1* (n = 12); in group E1_KO, *TMEM138* (n = 5), *CYB561A3* (n = 11), *DDB1* (n = 11)). (g) CRISPRi of E1 inhibits the gene expression of *CYB561A3* and *TMEM138* based on RNA-Seq data. The top 10 differentially expressed genes were labeled, P was calculated by Wald's test with multiple testing correction in DESeq2. (h) Volcano plot showed that CRISPR-mediated deletion of E1 reduces the gene expression of *CYB561A3* and *TMEM138*. The top 10 differentially expressed genes were labeled, P was calculated by Wald's test with multiple testing correction in DESeq2. (i) Gene ontology analysis of RNA-Seq data showed CRISPRi of E1 affects the expression of genes in pigmentation-related pathways. (j) Gene ontology analysis of RNA-Seq data showed CRISPR-mediated deletion of E1 affects the expression of genes in pigmentation-related pathways. Data were presented as mean \pm SEM. ns p > 0.05.

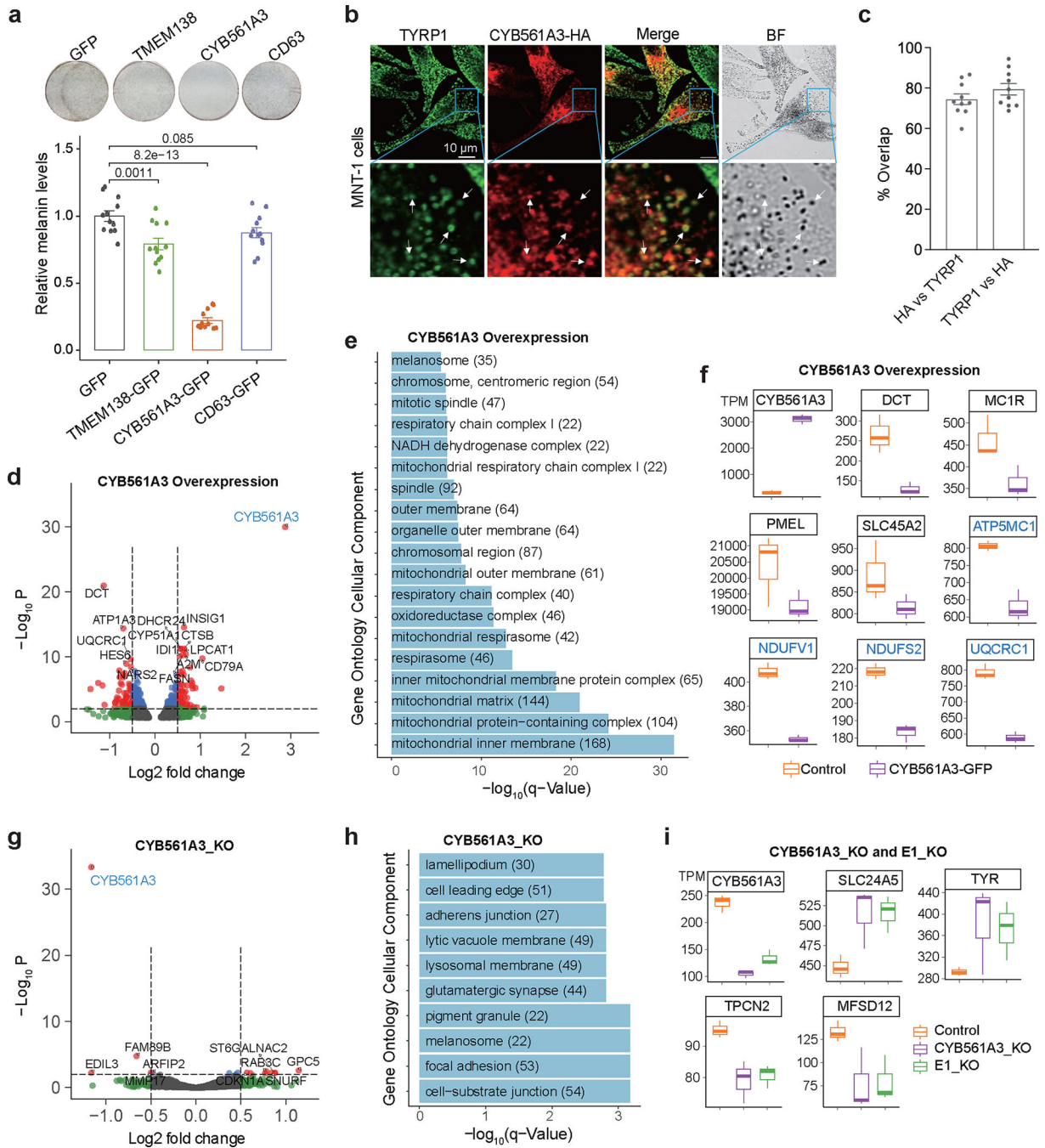


Fig. 7: CYB561A3 affects melanin levels in MNT-1.

(a) Overexpression of CYB561A3 significantly decreases melanin levels in MNT-1. Top panel shows photos of pigmentation levels of MNT-1 on the bottom of a 24-well plate. The MNT-1 were first treated with 150 μ M phenylthiourea (PTU, inhibits the biosynthesis of melanin) for 9 days and then infected with lentivirus encoding GFP, TMEM138-GFP, CYB561A3-GFP or CD63-GFP for 7 days. CD63-GFP is a negative control which does not affect pigmentation. The p-values are calculated using two-sided Tukey's test with adjustments for multiple comparisons ($n = 12$). (b) Confocal images of MNT-1

expressing CYB561A3-HA and immunostained with antibodies against the melanosomal marker TYRP1 (green) and HA (red). Scale bar: 10 μ m. Bottom images represent the enlarged areas shown in blue boxes. Arrows point to regions of overlap (yellow) between CYB561A3-HA and TYRP1-positive cellular structures. Three independent experiments. (c) Quantification of the overlap between CYB561A3-HA and TYRP1 in MNT-1 (n = 10 cells from 3 independent experiments). (d) Volcano plot showing differentially expressed genes in CYB561A3-overexpressed MNT-1. The top 10 most differentially expressed genes were labeled. P was calculated by Wald's test with multiple testing correction in DESeq2. (e) KEGG pathway analysis showed overexpression of CYB561A3 affects the expression of genes related to mitochondrial respiration and melanin production. (f) Overexpression of CYB561A3 affects the expression of genes related to melanosome and mitochondria function (n = 3). Genes involved in pigmentation were colored in black, and genes involved in mitochondrial function were colored in blue. (g) Volcano plot of differentially expressed genes in *CYB561A3*-knockout MNT-1. The top 10 differentially expressed genes were labeled, P was calculated by Wald's test with multiple testing correction in DESeq2. (h) GO analysis showed that *CYB561A3*-knockout affects melanogenesis-related pathways. (i) Both knockout of *CYB561A3* and deletion of enhancer E1 affect the expression of genes related to melanin production. Listed genes have p-values less than 0.05 based on DESeq2 (n = 3). For boxplots, central lines are median, with boxes extending from the 25th to the 75th percentiles. Whiskers further extend by ± 1.5 times the interquartile range from the limits of each box. Data were presented as mean \pm SEM.